Examining the low-voltage fast seizure-onset and its response to optogenetic stimulation in a biophysical network model of the hippocampus

Liyuan Zhang[1], Zhiyuan Ma[1], Ying Yu[2], Bao Li[1], Shuicai Wu[1], Youjun Liu[1*] and Gerold Baier[3*#]

1 Department of Biomedical Engineering, Faculty of Environment and Life, Beijing University of Technology, Beijing, 100124, China

2 School of Engineering Medicine, Beihang University, Beijing 100191, China

3 Cell and Developmental Biology, University College London, London, WC1E 6BT, United Kingdom

Corresponding Authors: Youjun Liu: lyjlma@bjut.edu.cn Gerold Baier: g.baier@ucl.ac.uk

# YL and GB contributed equally to this work.

Abstract: Low-voltage fast (LVF) seizure-onset is one of the two frequently observed temporal lobe seizure-onset patterns. Depth electroencephalogram profile analysis illustrated that the peak amplitude of LVF onset was deep temporal areas, e.g., hippocampus. However, the specific dynamic transition mechanisms between normal hippocampal rhythmic activity and LVF seizure-onset remain unclear. Recently, the optogenetic approach to gain control over epileptic hyper-excitability both in vitro and in vivo has become a novel noninvasive modulation strategy. Here, we combined biophysical modeling to study LVF dynamics following changes in crucial physiological parameters, and investigated the potential optogenetic intervention mechanism for both excitatory and inhibitory control. In an Ammon's horn 3 (CA3) biophysical model with light-sensitive protein channelrhodopsin 2 (ChR2), we found that the cooperative effects of excessive extracellular potassium concentration of parvalbumin-positive (PV+) inhibitory interneurons and synaptic links could induce abundant types of discharges of the hippocampus, and lead to transitions from gamma oscillations to LVF seizure-onset. Simulations of optogenetic stimulation revealed that the LVF seizure-onset and morbid fast spiking could not be eliminated by targeting PV+ neurons, whereas the epileptic network was more sensitive to the excitatory control of principal neurons with strong optogenetic currents. We illustrate that in the epileptic hippocampal network, the trajectories of the normal and the seizure state are in close vicinity and optogenetic perturbations therefore may result in transitions. The network model system developed in this study represents a scientific instrument to disclose the underlying principles of LVF, to characterize the effects of optogenetic neuromodulation, and to guide future treatment for specific types of seizures.

Key words Low-voltage fast seizure-onset, hippocampus, optogenetic stimulation, parvalbumin-positive inhibitory neurons, rhythmic oscillation

Introduction

Temporal lobe epilepsy (TLE) is the most common medically intractable focal epilepsy in adults. It is associated with recurrent seizures that arise from temporal lobe areas such as the hippocampus. Clinical evidence showed that TLE is characterized by 5-9 Hz lateralized rhythmic theta activity or 2-5 Hz lateralized rhythmic delta activity from ictal scalp-EEG data (Pelliccia et al. 2013). According to their onset patterns, seizures in TLE can be classified as hypersynchronous (HYP) and low-voltage fast (LVF) activity (Shiri et al. 2015), and LVF has been demonstrated to be the most common focal-onset seizure pattern according to clinical data and experimental evidence (De Curtis and Avoli 2016). LVF is usually characterised by elevated frequency (Lee et al. 2000) and initially low amplitude, and is regarded as an electrophysiological hallmark of the epileptogenic zone. In vitro intracellular recordings indicated that LVF seizure-onset is initiated by hypersynchronous interneurons, mainly parvalbumin-positive (PV+), which induce the postsynaptic activation of γ-aminobutyric acid type A ($GABA_A$) receptors on principal cells, and depolarization block of interneurons (Avoli et al. 2011 & 2016). Rhythmic oscillatory activity is also a hallmark of normal neuronal network function in certain brain regions, especially the hippocampus. The main rhythms of the hippocampus are low theta (4-12Hz) to high gamma (30-90Hz). Hippocampal theta and gamma oscillation are important for learning and memory, and protection of cell assemblies (Bartos et al. 2007). They are believed to represent a fundamental mechanism to transfer information across spatial and temporal scales (Segneri et al. 2020). The neural circuits of the hippocampus are extremely complex, with electrophysiological experiments (Gafurov and Bausch 2013; Dugladze et al., 2013; Marafiga et al. 2021) revealing contributions of many types of neurons including pyramidal cell and interneurons to normal or epileptic rhythmic oscillatory dynamics, respectively. Numerous computational works have attempted to disentangle the underlying microscopic (Du et al. 2016; Ferguson et al. 2017; Howe et al. 2020; Mushtaq et al. 2021; Olteanu et al. 2021) and mesoscopic (Oprisan et al. 2018; Segneri et al. 2020) biophysical mechanisms. Pioneering electrophysiological experiments showed that the Ammon's horn 3 (CA3) region displayed a "scale-free" functional topology (Bonifazi et al. 2009). These authors showed that GABAergic neurons with features of high output functional connectivity underly hub network function (Picardo et al. 2011). We thus constructed a computational biophysical network of the CA3 region considering the hub role of GABAergic neurons (with PV+ expression) to investigate the dynamical mechanism of the transition between hippocampus normal rhythmic and LVF activity.

Diverse techniques including electrophysiology, nuclear magnetic resonance, and optogenetics have provided new ways to study the structure and function of neural circuits (Boyden et al. 2005) and intervene in neural behaviors (Zhang H et al. 2020; Yu et al. 2021). In the field of therapeutic strategies for medically intractable epilepsy, including deep brain stimulation (DBS), responsive neurostimulation (RNS), transcranial direct current stimulation (tDCS) (Zhang L et al. IEEE. 2020), transcranial magnetic stimulation (TMS) and optogenetic stimulation are increasingly being considered to reduce seizure frequency (Krook-Magnuson et al. 2013). Notably, optogenetics using light to modulate neural circuits via viral transduction of protein channels, has been shown to control experimental spontaneous seizures (Tønnesen et al. 2009; Krook-Magnuson et al. 2014). The biggest advantages of optogenetic techniques is their ability to target genetically defined neuronal populations. Theoretical research has explored the underlying principles of optogenetic neural stimulation of pyramidal neuron (Foutz et al. 2012), particularly in channelrhodopsin-2 (ChR2)-expressing neurons (Nikolic et al. 2009; Talathi et al. 2010; Stefanescu et al. 2013; Renault et al. 2018). In terms of optogenetic control for epilepsy, Rezvani-Ardakani et al. (2020) designed the control method of fixed time integral super twisting sliding mode and tested the reliability on a pyramidal model. In macroscopic models, Shen et al. (Shen et al. 2022) created six smart optogenetic strategies for generalized periodic epileptiform discharges. These results facilitate our understanding of optogenetic stimulation in epilepsy and help to guide clinical practice. Making use of optogenetics to investigate the role of neuron populations in epilepsy, on-demand stimulation was employed to excite inhibitory interneurons (Krook-Magnuson and Soltesz 2015). Krook-Magnuson et al. demonstrated PV+ interneurons as a potential therapeutic target and improved understanding of mechanisms of ictogenesis (Krook-Magnuson et al. 2013). However, PV+ neuron populations also have the capability of inducing seizures by introducing aberrant synchrony (Jiruska et al. 2013). In particular, researchers found that spontaneous seizure-like events induced by optogenetic activation of interneurons demonstrated LVF (Shiri et al. 2016). Motivated by these studies, we investigate the transition dynamics between hippocampal normal rhythmic activities and typical LVF-seizure onset, and test hypotheses about optogenetic stimulation of both principal cells and interneurons to disclose the mechanism underlying behavioral phenomena.

Methodology

Biophysical computational network model

We adopt the computational model proposed by Olufsen et al (2003) to describe firing behavior of a hippocampal pyramidal cell. The membrane potential of a single cell obeys the following differential equations:

$$\begin{cases} C_m \frac{dV}{dt} = g_{Na} m_\infty(V)^3 h(V_{Na} - V) + g_K n^4 (V_K - V) + g_L (V_L - V) + I \\ \frac{dh}{dt} = \frac{h_\infty(V) - h}{\tau_h(V)} \\ \frac{dn}{dt} = \frac{n_\infty(V) - h}{\tau_n(V)} \end{cases} \quad (1)$$

with $x_\infty(V) = \alpha_x(V)/\big(\alpha_x(V) + \beta_x(V)\big)$ for $x = \mathrm{m, h}$ or n, $\tau_x(V) = 1/\big(\alpha_x(V) + \beta_x(V)\big)$ for $x = h$ or n. The respective parameter values of the pyramidal model are $C_m = 1\mu F/cm^2$, $g_{Na} = 100mS/cm^2$, $g_K = 80mS/cm^2$, $g_L = 0.1mS/cm^2$, $V_{Na} = 50mV$, $V_K = 100mV$ and $V_L = -67mV$. More details about the rate functions are available in Ref. Olufsen et al. 2003 and Kopell et al. 2010.

For PV+ interneuron, we use the mathematical model created by Wang and Buzśaki (1996). The main equations are as in the pyramidal cell model, where the equation for $\tau_x(V)$ is replaced by $\tau_x(V) = 0.2/\big(\alpha_x(V) + \beta_x(V)\big)$. The parameters are $C_m = 1\mu F/cm^2$, $g_{Na} = 35mS/cm^2$, $g_L = 0.1mS/cm^2$, $V_{Na} = 55mV$, $V_K = -90mV$ and $V_L = -65mV$. Here g_K is a bifurcation parameter, ranging from 5 to 105mS/cm^2. Other function-settings are available in Wang and Buzśaki (1996).

The external inputs I in Eq. (1) for cells are divided into deterministic and stochastic components. The deterministic current for a pyramidal cell is $I_{PY} = 2\mu A/cm^2$ for the analysis of the two-dimensional parameter space; it varies from $0.5\mu A/cm^2$ to $3\mu A/cm^2$ for the three-dimensional parameter space, and for a PV+ cell is $I_{PV+} = 0.3\mu A/cm^2$. We adopt Kopell et al's approach (2010) for the stochastic component for each cell. Details of the parameter setting are in Ref. Kopell et al. 2010.

We employ the chemical synaptic model of Ermentrout and Kopell (1998) for the neural network. The synaptic gating variable s obeys to the principle $\frac{ds}{dt} = \frac{\rho(V)(1-s)}{\tau_R} - \frac{s}{\tau_D}$ where ρ is a Heaviside function with the form $\rho(V) = \big(1 + tanh(V/4)\big)/2$. Therefore, the synaptic current from neuron i to neuron j has the form $g_{ij} s_i(t)\big(V_{rev} - V_j\big)$ where g_{ij} is the maximum conductance of the synapse. We set the synaptic strength between pyramidal cell and PV+ cell to

$g_{PY\to PV+} = 0.001 mS/cm^2$, $g_{PY\to PY} = 0.0001 mS/cm^2$, $g_{PV+\to PY} = 0.001 mS/cm^2$ and $g_{PV+\to PV+} = 0.03 mS/cm^2$. In simulations, we found that the rise and decay time constants τ_R and τ_D affect the neuronal behavior. Here we regard the proportion of τ_R and τ_D from PV+ neurons as a crucial parameter. For an α-amino-3-hydroxy-5-methyl-4-isoxazole-propionicacid (AMPA) type synapse, we set $\tau_R = 0.1$, $\tau_D = 3$ and $V_{rev} = 0 mV$. For a $GABA_A$ type synapse, $V_{rev} = -80 mV$. The proportion coefficient K_τ is defined as $\tau_R/\tau_D = K_\tau/(30K_\tau)$, ranging from 0.3 to 3.9 (Ermentrout and Kopell, 1998).

Because the CA3 network demonstrates scale-free topology, we construct a scale-free biophysical network of CA3 with pyramidal cells $N_{PY} = 800$ and PV+ cells $N_{PY} = 200$. Fig. 1(a) shows the schematic diagram of the network. Therein, PV+ cells have more links with other cells. Scale-free properties have been proposed for studies on large-scale brain networks (Gadhoumi et al. 2015; Stam and Reijneveld 2007; Emerson et al 2019). We organize the network by assigning a probability $P(k)$ that a node in the network interacts with k other nodes and this probability decays as a power-law, obeying a Poisson distribution with probability $\mathrm{P}(k) = (\lambda^k \exp(-\lambda))/k!$, where k represents the number of links and λ denotes the decay exponent. We begin with a small number of nodes (m_0), and then add new nodes with $m \le m_0$ edges (Barabási and Albert 1999; Barabási 2009). The probability that an existing node i connects with a new node depends on its connectivity k_i. According to this rule, the network will expand to a scale-free network with $\mathrm{t} + m_0$ and $m\mathrm{t}$ links (Barabási and Albert 1999). Here we show an example network with $m_0 = 5, m = 5$ considering PV+ cells as the hub nodes. In our network configuration, the scale-free link matrix is $\mathbf{A} = (a_{ij})_{(N_{PY}+N_{PV+})\times(N_{PY}+N_{PV+})}, \mathrm{i} = 1, \dots, N_{PY} + N_{PV+}, \mathrm{j} = 1, \dots, N_{PY} + N_{PV+}$. If node i connects with node j, $a_{ij} = a_{ji} = 1$, else $a_{ij} = a_{ji} = 0$ (Fig. 1(b)). We reorder the link matrix $\mathbf{A}$ such that node No.1 of PV+ cells has maximum links, No. 2 has the second most links, and so on. The last pyramidal cell has the smallest number of links. The coupling strength matrix $\mathbf{C}$ is $\mathbf{C} = \boldsymbol{A}_{new} \times \begin{bmatrix} \boldsymbol{E}_{N_{PV+}\times N_{PV+}} g_{PV+\to PV+} & \boldsymbol{E}_{N_{PV+}\times N_{PY}} g_{PV+\to PY} \\ \boldsymbol{E}_{N_{PY}\times N_{PV+}} g_{PY\to PV+} & \boldsymbol{E}_{N_{PY}\times N_{PY}} g_{PY\to PY} \end{bmatrix}$ where $\boldsymbol{A}_{new}$ is the reordered form of $\mathbf{A}$, and $\mathbf{E}$ is a matrix with all elements equal to one.

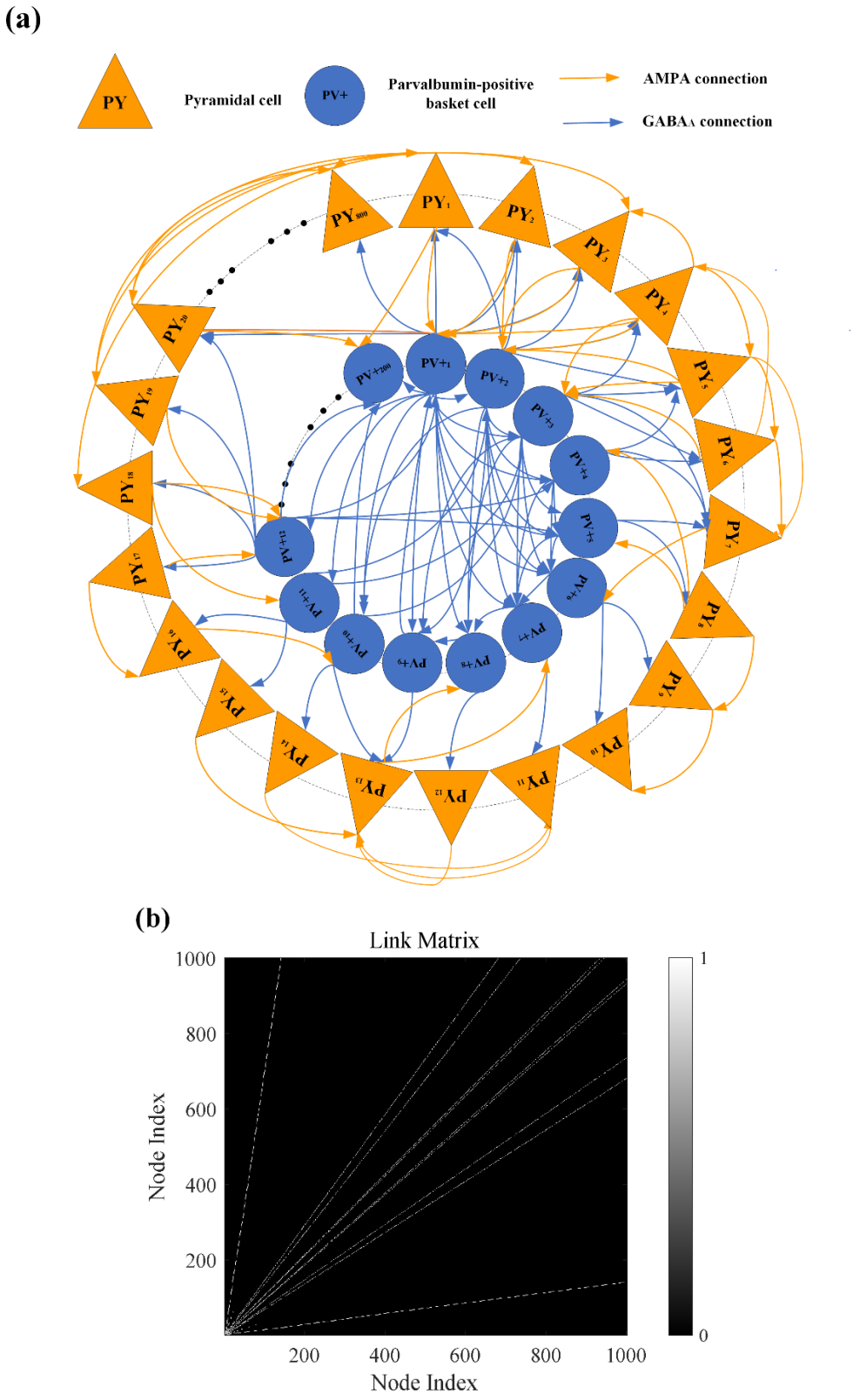

Figure 1. The basic configuration of the biological hippocampal network model for CA3. (a) presents a sketch of cell relationships. The orange pyramids (from No. 1 to No.800) and arrows indicate pyramidal cells and AMPA type links, respectively. The dark blue circles (from No.1 to No.200) and arrows denote PV+ cells and $GABA_A$ links, respectively. Cells connect with each other according to the reordered form

of the original link matrix, where the PV+ cells own the maximum links. (b) illustrates the original link matrix **A**. We calculate the degree of **A** and then reorder it.

The optogenetic model based on ChR2 expression

In our work, we implement the light-sensitive ChR2 expression protein in pyramidal and PV+ cells, respectively. ChR2 is a subfamily of blue light gated-cation opsins, which can be activated by blue light with wavelength 470nm (Nagel et al. 2003). From a modelling perspective, there are two transition rate models, the 3-state model and the 4-state model, which imitate wild-type ChR2 photocurrent kinetics (Nikolic et al. 2009). In the study by Stefanescu et al. (2013), it is pointed out that the 4-state model could capture the bi-exponential photocurrent decay characteristic. Therefore, we chose the 4-state model for the benefit of enhanced capacity of dynamical behavior and increased complexity of the network model. Indeed, this kind of optogenetic stimulation has been used to control neural synchrony (Talathi et al. 2010) in a unidirectionally coupled network assembled from the model of Wang and Buzśaki (1996). Further, a network with 800 excitatory pyramidal cells and 200 inhibitory neurons was used to help guide optogenetics experiments (Tiesinga et al. 2012). They constructed a network with an unstable state which could be perturbed by external optogenetic stimulation. Recently, this optogenetic stimulation approach is also used for the analysis of neural activity patterns (Zhang H et al. 2020) and regulation of Parkinsonian neural network (Yu et al. 2021). In line with these results on optogenetic stimulation on neuronal networks, we introduce the ChR2 channel modelled 4 states to our network model. Here we modeled ChR2 with four states: two closed states (C_1, C_2), and two open states (O_1, O_2), c.f. Fig. 2(b). In the transition model, ChR2 could be excited from the baseline closed state C_1 to an open state O_1 by absorption of a photon of blue light with wavelength of about 470nm (Fig. 2(a)). If ChR2 is in the excited state O_1, it can decay back to a closed state C_1 or transition to another open state O_2. ChR2 in state O_2 can either return to state O_1 or decay back to a closed state C_2. Finally, state C_2 can either be photoexcited back to O_2 or transit to C_1 (Foutz et al. 2012). A sketch of the transitions among the four states is shown in Fig. 2(b).

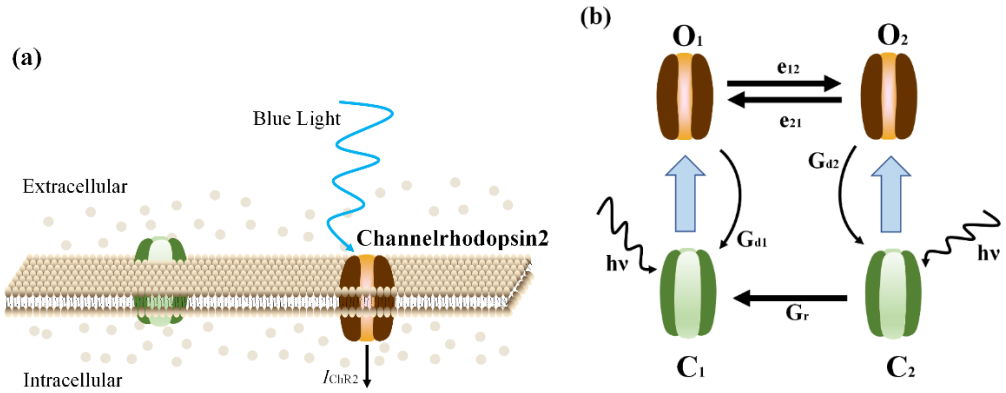

Figure 2. Optogenetic transition model. (a) indicates blue light that is absorbed by ChR2, opening the extracellular channel gate and permitting a photocurrent I_{ChR2} into the cell. The brown protein molecules show open states, and the green protein molecules switch to closed state. The small circles are phospholipid molecules which constitute phospholipid bilayer. (b) represents the 4-state transition model with two open states (O_1 and O_2) and two closed states (C_1 and C_2). Channels can transition between four states with rate constants (G_{d1}, G_{d2}, G_r e_1 and e_2).

The ChR2 photocurrent kinetics can be implemented via the following equations (Talathi et al., 2010):

$$\begin{cases} \frac{do_1}{dt} = P_1 s(1 - c_1 - o_1 - o_2) - (G_{d1} + e_{12})o_1 + e_{21}o_2 \\ \frac{do_2}{dt} = P_2 s c_2 + e_{12}o_1 - (G_{d2} + e_{21})o_2 \\ \frac{dc_2}{dt} = G_{d2}o_2 - (P_2 s + G_r c_2) \\ \frac{ds}{dt} = \frac{S_0(\theta) - s}{\tau_{ChR2}} \\ c_1 + c_2 + o_1 + o_2 = 1 \end{cases} \quad (2)$$

where c_1, c_2, o_1 and o_2 are the fraction of ChR2 molecules in each of the four states C_1, C_2, O_1 and O_2, respectively. P_1 and P_2 are the maximum excitation rates of the first and second closed state. G_{d1}, G_{d2}, e_1 and e_2 are the transition rate constants. G_r is the recovery rate of the first closed rate after the light pulse is turned off. $S_0(\theta) = 0.5(1 + \tanh(120(\theta - 1)))$ is a sigmoid function where $\theta(t) = \sum_i \Theta(t - t_{i_{on}})\Theta(t - t_{i_{off}})$ denotes the optogenetic stimulation protocol. $\Theta(x) = \begin{cases} 1 & x > 0 \\ 0 & x \leq 0 \end{cases}$ is the Heaviside function. $t_{i_{on}}$ and $t_{i_{off}}$ represent the onset and offset time of the i_{th} optogenetic stimulation pulse, respectively. τ_{ChR2} is the activation time constant of the ChR2 channel. Finally, the ChR2 photocurrent can be described as $I_{ChR2} = Vg_1(o_1 + \gamma o_2)$ where V can denote the membrane potential of either a pyramidal cell or a PV+ cell. For the empirical parameters we refer the reader to Ref. Stefanescu et al. 2013. Employing the wild-type ChR2 model,

we set $\left\{P_1 = 0.0641ms^{-1}, P_2 = 0.06102ms^{-1}, G_{d1} = 0.4558ms^{-1}, G_{d2} = 0.0704ms^{-1}, e_{12} = 0.2044, e_{21} = 0.009, G_\gamma = \frac{1}{10700}ms^{-1}, \gamma = 0.0305\right\}$ (Stefanescu et al., 2013), and regard $g_1$as bifurcation parameter.

All simulations were done in MATLAB, version R2020a (https://ww2.mathworks.cn/en/).

Results

Dynamical features of the biophysical network model

Based on the pioneering studies of (Kopell et al. 2010; Taxidis et al. 2013; Ferguson et al. 2017; Evangelista et al. 2020; Olteanu et al. 2021), we construct a PV+ cell dominated network with scale-free topology to study dynamical features of the hippocampal network. We first look at the influence of parameter changes on this topology. Fig. 3(a1) and (a2) illustrate the time series of a pyramidal cell and a PV+ cell with parameters $g_K = 9\ mS/cm^2$ and $K_\tau = 0.3$. The power spectra in Fig. 3(b1) and (b2) illustrate a dominant frequency for the two cells to lie mainly in the gamma band (about 30Hz). To demonstrate synchronous activities, we provide the spike raster diagram of the network in Fig. 3(c). All cells fire synchronously at the gamma band frequency. This confirms that hippocampal rhythmic activity can be produced by pyramidal-interneuronal network gamma (PING). Both excitatory and inhibitory cells are involved, with both types of cells firing synchronously at or near the population frequency in PING (Kopell et al. 2010). Considering the conclusion proposed in Börgers and Kopell, 2003, the PING mechanism works because the pyramidal cell fires around gamma frequency after receiving external input. Then, the pyramidal cell triggers the response of the PV+ cell, in turn, the pyramidal cell is suppressed and the firing time of the pyramidal cell is ahead of the PV+ cell. Strongly driven pyramidal cells participate in every cycle, and synapses between PV+ cell and pyramidal cell are strong enough to approximately synchronize the PV+ and the pyramidal cells.

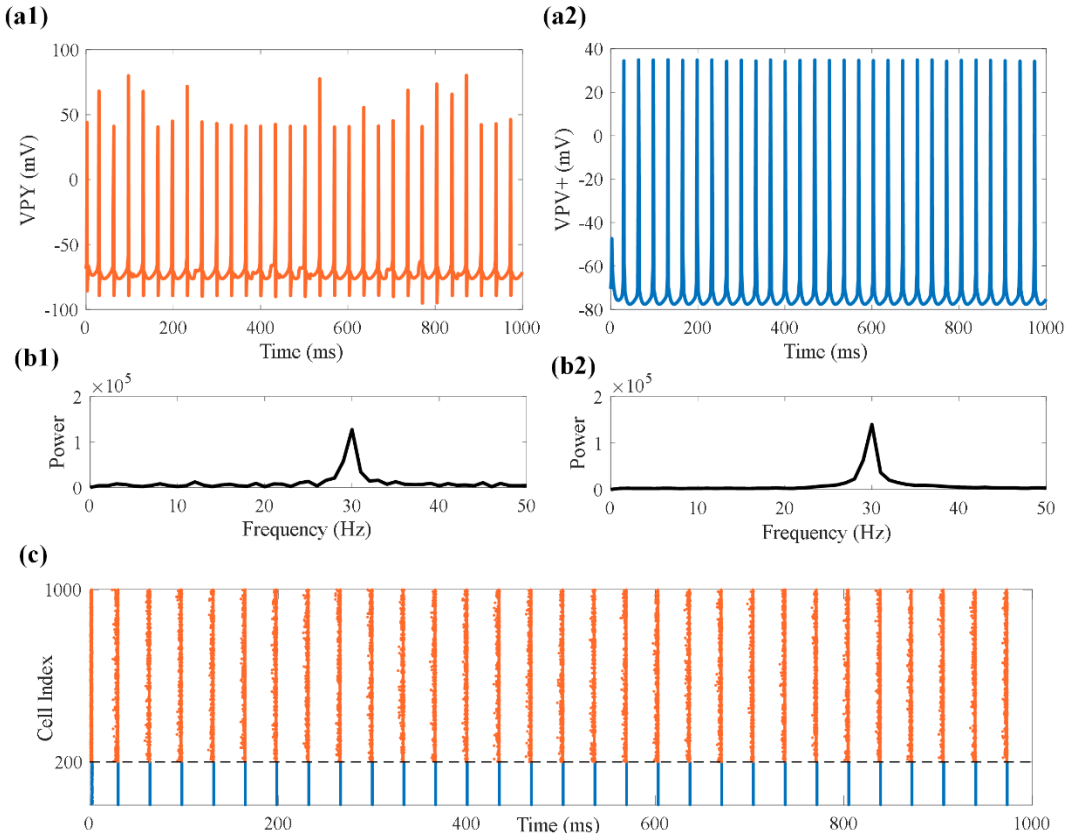

Figure 3. Illustration of a rhythmic oscillation for the hippocampal network. (a1) and (a2) are time plots for a pyramidal cell and a PV+ cell. (b1) and (b2) are their respective power spectra. (c) shows the spike raster diagram of the network where dark blue dots for index 1 to 200 represent spikes of PV+ cells and the orange dots are spikes of pyramidal cells.

The basic analysis in Fig. 3 demonstrates that the network has the capability to produce normal rhythmic activity in the hippocampus by regulating the gate variable of potassium and synaptic decay and rise time constant in PV+ cell, respectively. When increasing g_K to 90 mS/cm^2 and K_τ to 2.7, the pyramidal cells exhibit very fast spiking activities (Fig. 4(a1)) with dominant frequency of around 500Hz (Fig. 4(b1)). It is common to observe interictal epileptic high-frequency oscillations (HFOs) in focal epilepsy, and HFOs are thought to reflect pathological activity of neuronal networks (Engel et al. 2009). According to the oscillation frequency, HFOs can be categorized as ripples (80-200Hz) and fast ripples (250-500Hz), respectively (Lévesque et al. 2018). Therefore, pyramidal cells exhibit fast ripple activity under increasing intracellular concentration of potassium ions and the synaptic response of a PV+ cell, respectively. This illustrates the conclusion drawn by Demont-Guignard (2012): fast ripples might be generated by a small volume of brain

tissue that contains hyperexcitable pyramidal neurons. Under these conditions, we can produce a typical LVF seizure-onset in PV+ cells (Fig.4 (a2) as $g_K = 90\ mS/cm^2$ and $K_\tau = 2.7$). In the power spectrum in Fig. 4(b2), we observe a new slow main frequency component below 10Hz in addition to the ripple frequency. The detail drawn from 530ms to 570ms reveals a very fast rhythmic oscillation component at about 400Hz. It has been reported that ripples can occur during the pre-ictal phase of LVF seizures (Lévesque et al. 2012), although the strength of the relationship between ripples and LVF seizures decreases with disease progression (Lévesque and Avoli 2019). Hence, it is important to find a fast ripple component in the network with LVF seizure-onset. Both pyramidal cells and PV+ cells maintain synchronous activities, as demonstrated in the raster diagram Fig. 4(c). It shows that the slow component is produced by interneuron firing whereas the fast spiking pyramidal cells create the ripple frequency.

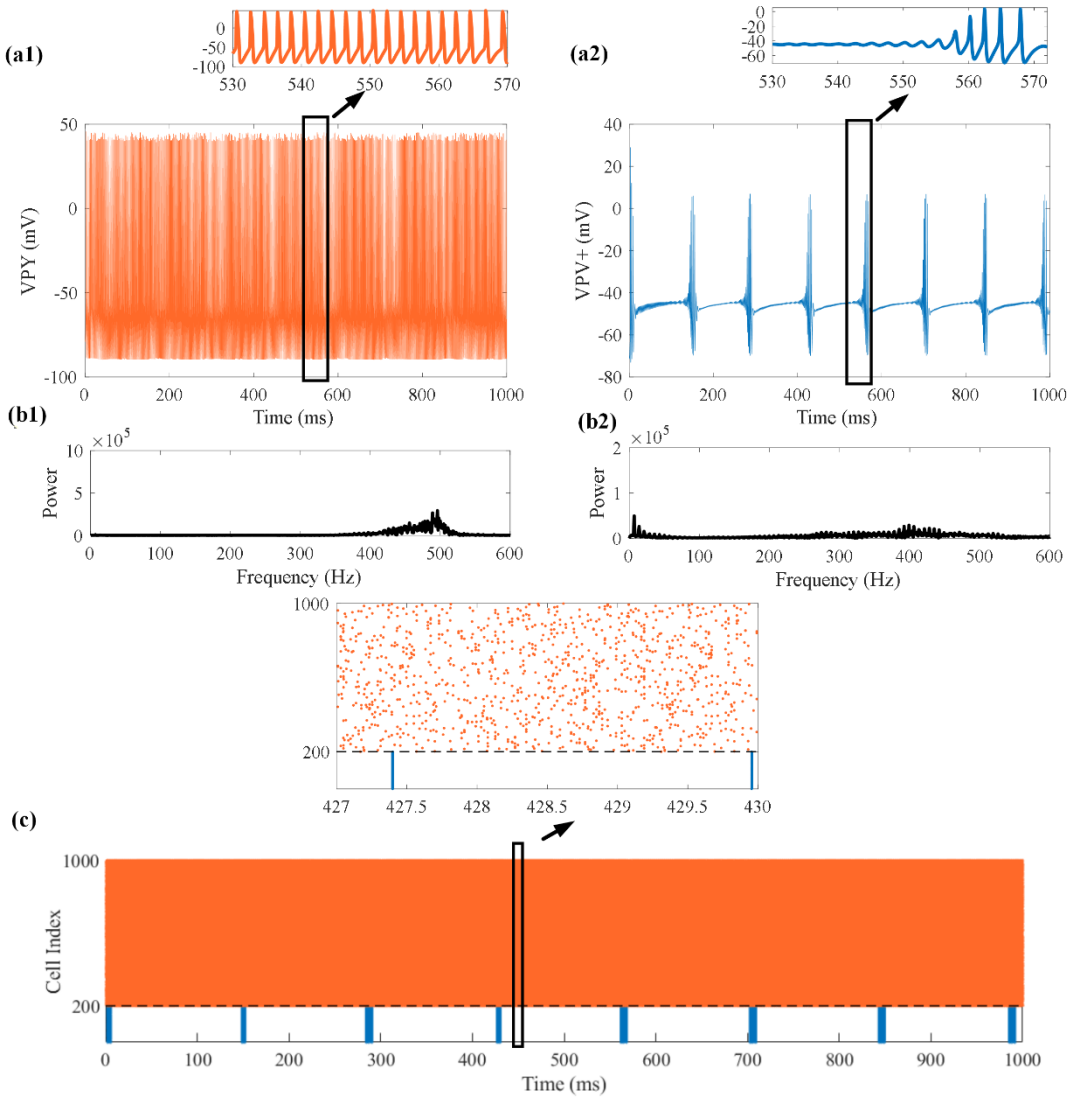

Figure 4. Demonstration of an epileptic oscillation for the hippocampal network. (a1) and (a2) represent time plots for a pyramidal cell and a PV+ cell, respectively. Details are shown from 530ms to 570ms. (b1) and (b2) are their respective power spectra. (c) is the spike raster diagram of the network. Above it, a detail is shown from 427ms to 430ms.

We then examined the phase space portraits with membrane potentials and activation variable of potassium in the rhythmic gamma state and in the morbid state, respectively. In the phase space diagram of a pyramidal cell in Fig. 5(a1), we see that the normal gamma rhythmic oscillation (red) is well separated from the fast spiking trajectory (blue), which suggests that moderate random perturbations alone will not result in transitions between the two states. A similar result can be found in Fig. 5(b2) for a PV+ cell. The LVF state (blue) has a very focused attractor which induces an oscillation in small amplitude with a tube-like structure. It is implied that a supercritical Hopf bifurcation occurs during the transition from the rhythmic state to the LVF state (Saggio et al. 2020; Zhang L et al. Chaos 2020). To be more specific, we investigate the interspike interval (ISI) bifurcation diagrams for pyramidal cells and PV+ cells, respectively. It is observed from Fig. 5(a2) that the pyramidal cells show gamma oscillation activities before reaching the bifurcation point P1 and then transits to the spiking and bursting alternating state after undergoing a dynamical bifurcation, and eventually arrive at the fast spiking state by crossing point P2. A similar bifurcation situation is found in Fig. 5(b2) for PV+ cells. By increasing the crucial parameter K_τ, we successively find the gamma oscillation state, the spiking and bursting alternating state (cross point P1) and the seizure bursting state (cross point P2). These examples of dynamical bifurcation analysis show the qualitative state transitions, but we wish to describe state transitions driven by crucial parameters quantitively.

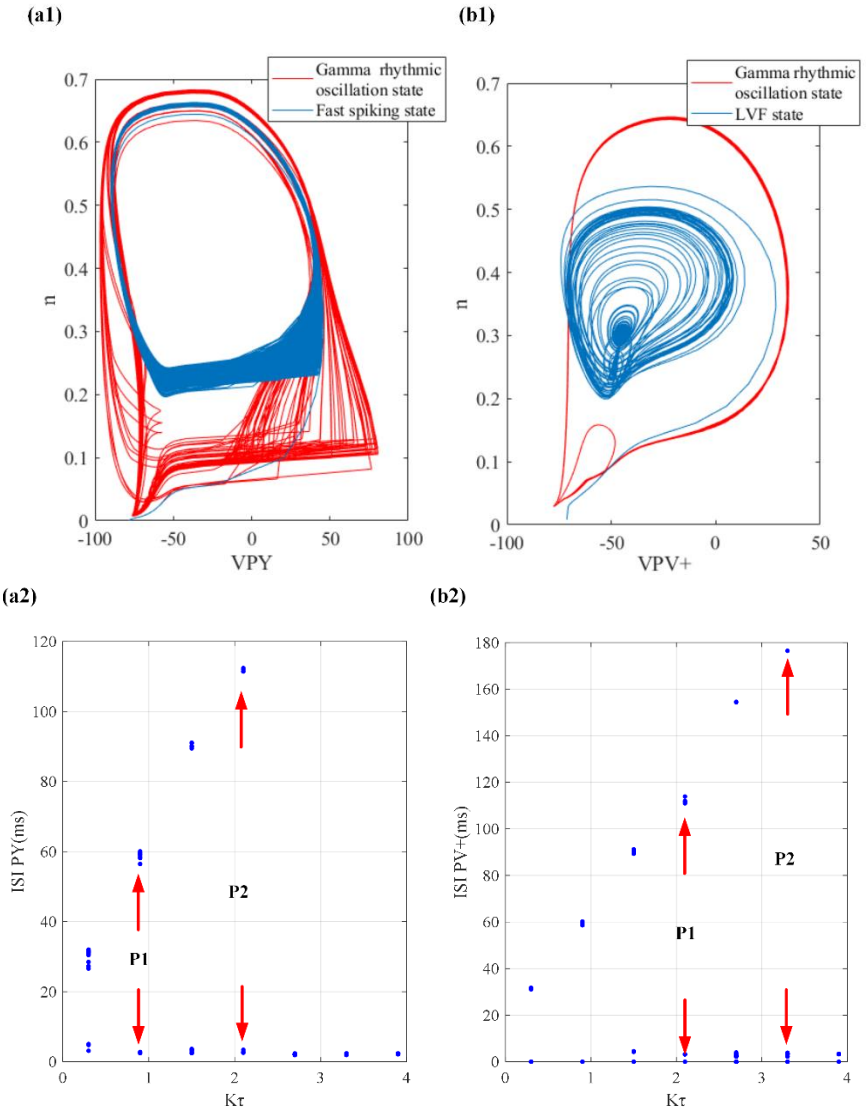

Figure 5. Analysis of dynamical transitions for pyramidal cells and PV+ cells, respectively. (a1) Phase space portraits with membrane potentials and activation variable of potassium ions. trajectories of pyramidal cell for gamma rhythmic state (red curve) and fast spiking state (dark blue curve), respectively. (b1) Phase space portraits of gamma rhythm (red curve) and LVF state (dark blue curve) of a PV+ cell, respectively. (a2) and (b2) are illustrations of ISI bifurcation diagrams for pyramidal cells and PV+ cells, respectively. P1 and P2 with red arrows indicate the bifurcation points in both (a2) and (b2).

Based on the dynamical analysis above, we explored the influence of crucial parameters including g_K and K_τ on the network dynamics in terms of the neuronal state. Also, we consider the external input (Franaszczuk et al. 2003) of pyramidal cells to construct a three-dimensional parameter space. The procedure of exploring the influence of the external input to PV+ cells in the parameter diagram is similar to before (not shown). We take the former one as an example. We

consider five states: the spiking rhythmic state (1), the spiking and bursting alternating state (2), fast spiking (3), the epileptic bursting and fast spiking alternating state (4) and plain epileptic bursting (5). We first start with a two-dimensional parameter space. In Fig. 6(a1), (a2), (b1) and (b2), we see that both pyramidal cells and PV+ cells are in the spiking state with dominant frequency in the gramma band when K_τ is small enough and g_K changes from 9 to 75 mS/cm^2. By increasing K_τ and fixing g_K, we find that pyramidal cells transit to the spiking and bursting alternate state (with dominant frequency less than 50Hz as shown in Fig. 6(b1)), while PV+ cells remain in the spiking state. If we continue increasing K_τ while keeping g_K unchanged, we obtain the fast spiking state (with dominant frequency above 400Hz as shown in Fig. 6(b1)) in pyramidal cells, while PV+ cells have switched to the epileptic bursting and fast spiking alternate state (with dominant frequency between 200Hz to 300Hz, Fig. 6(b2)). Eventually, PV+ cells switch to the epileptic bursting state (with dominant frequency less than 30Hz, Fig. 6(b2)) when both g_K and K_τ are large enough. These observations verify that the synchronous, excessive PV+ interneuron discharge induces postsynaptic activation of $GABA_A$ receptors on pyramidal (principal) cells and interneurons undergoing a depolarization block as the extracellular concentration of potassium ion is elevated (involved in g_K). Finally, the hyperexcitable neuronal network generates LVF seizures (see e.g. Avoli et al. 2016). Specifically, the rhythmic gamma oscillation of the network is the dynamics in which the population of PV+ spikes depend on the decay time (involved in K_τ) of inhibitory postsynaptic potentials. The synaptic response is thus a crucial factor in determining the frequency of the rhythms (Kopell et al. 2010).

Next, we go to the three-dimensional parameter space shown in Fig. 6(c1) and (c2). When gradually increasing the external input of pyramidal cells (I_{PY}), the pyramidal cells demonstrate rhythmic spiking when K_τ is not big enough, but they then switch to the bursting alternating state or fast spiking state when increasing K_τ. When I_{PY} is big enough, the spiking rhythmic state disappears and the fast spiking state becomes the dominant state for pyramidal cells, Fig. 6(c1). In terms of PV+ cells, they demonstrate affluent state transitions (Fig. 6(c2)) by regulating I_{PY}. Similar to pyramidal cells, the PV+ cells also show rhythmic spiking and fast spiking when I_{PY} is set at small values. If we continue increasing I_{PY}, we either get the plain epileptic bursting state with a big g_K or the bursting alternating state with small g_K. Finally, the range of the plain epileptic bursting state is reduced when I_{PY} is big enough. In all, both the two-dimensional parameter space

with g_K and K_τ and the three-dimensional space with added I_{PY} provide multidimensional structural proofs for transitions which are essential to extract the relevant dynamical features of the network.

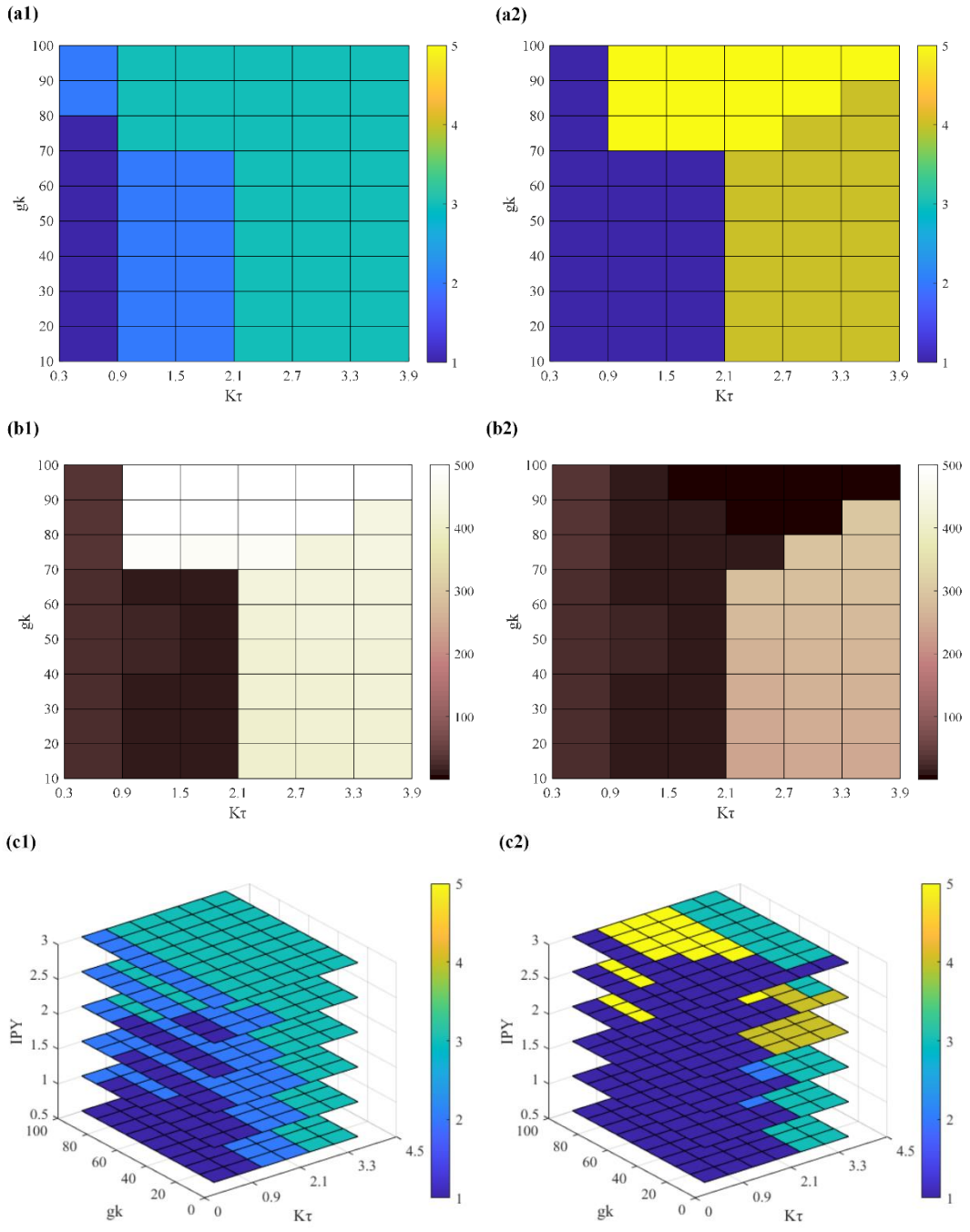

Figure 6. Parameter spaces of the dominant firing frequency for neuronal states in two and three dimensions. (a1) and (a2) are two-dimensional parameter (g_K and K_τ) diagrams for pyramidal cells and PV+ cells, respectively. The five states are the spiking rhythmic state (1), the spiking and bursting alternating state (2), fast spiking (3), the epileptic bursting and fast spiking alternating state (4) and plain epileptic bursting (5). Pyramidal cells occupy three states: rhythmic spiking state, spiking and bursting

alternating state, and the fast spiking state. PV+ cells display the rhythmic spiking state, epileptic bursting and fast spiking alternating state, and the epileptic bursting state. (b1) and (b2) are their corresponding dominant firing frequencies. (c1) and (c2) are three-dimensional parameter (g_K, K_τ and I_{PY}) diagrams for pyramidal cells and PV+ cells, respectively.

Testing the optogenetic stimulation effects on the hippocampal network

Optogenetic technology has been applied for the induction as well as the inhibition of seizures across a range of seizure and epilepsy models. Cell-type selective modulation of seizures has been designed as a new intervention strategy. Therein, an on-demand optogenetic strategy based on ChR2 expression has been applied in parvalbumin expressing cells in the experimental intrahippocampal kainite model of chronic TLE to inhibit seizures (Krook-Magnuson et al. 2013 & 2014). We therefore tested whether optogenetic stimulation controlling only PV+ cells could terminate LVF seizure-onset. There are numerous state transitions defined as 'seizure suppression', but in this section we look at how to switch from the fast spiking state of pyramidal cells and the plain epileptic bursting state of PV+ cells back to normal gamma oscillations with optogenetic stimulation.

As described above, parameter g_1 which determines the strength of photocurrent directly is regarded as the crucial bifurcation factor. Parameters of the hippocampal network were set to simulate LVF seizure-onset and fast-spiking activity. We consider the condition of low frequency (20Hz) optogenetic stimulation protocols with very short duration (2ms) following Stefanescu et al (2013). Stimulation is added at 200ms to all PV+ cells. From Fig. 7 (a1) we find that the firing activities of pyramidal cells are nearly unchanged, no matter whether g_1 is small or large. All demonstrate fast spiking (c.f. the detail in Fig. 7 (a2)). In contrast, PV+ cells exhibit stronger changes for various values of g_1, see Fig. 7 (b1). In the first trial (bottom), PV+ cells show a small response as the second light pulse arrives but then continue their intrinsic oscillation. In the second and third trials, cells demonstrate a stronger response to stimulation, including burst sequences. By increasing g_1 to 40 mS/cm^2, we observe that bursts in the second and third trial split into individual spikes. Further, spikes in the fifth trial have large depolarizations and form excitatory postsynaptic potentials (EPSPs).

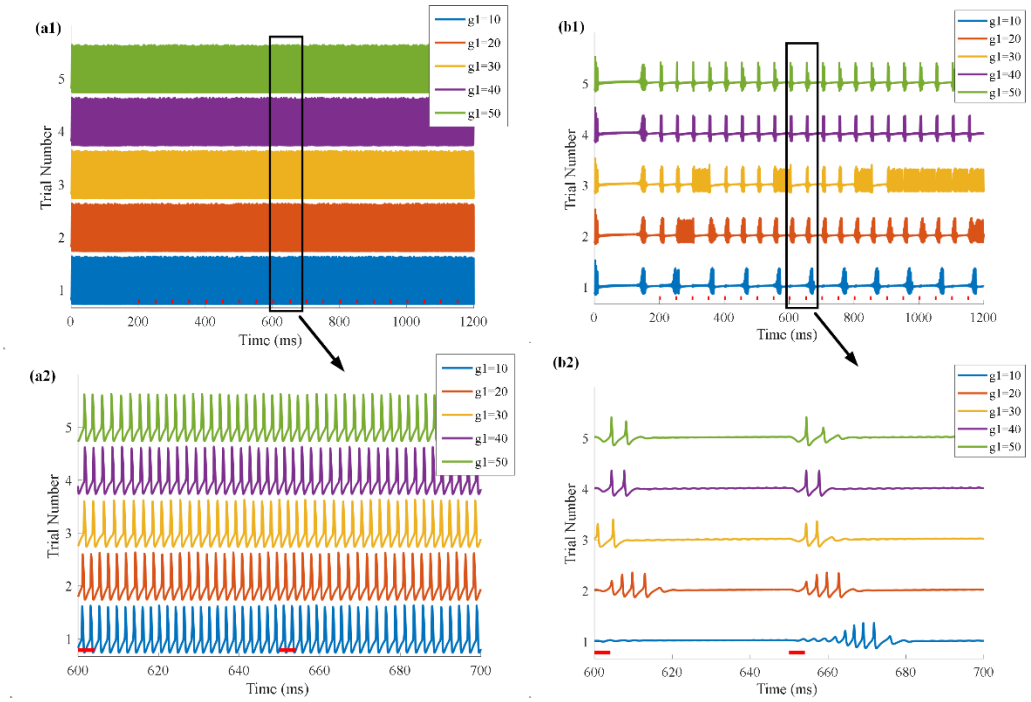

Figure 7. Time plots of pyramidal cell and PV+ cell under optogenetic stimulation on PV+ cells. The red rectangles denote light pulses. (a1) includes results (time series in dark blue, dark orange, yellow, purple and green) of five trials for a pyramidal cell corresponding to $g_1 = 10, 20, 30, 40$ and 50 mS/cm^2 and (a2) records details from 600ms to 700ms. (b1) and detail (b2) show the case of a PV+ cell.

To explore activities from a network point of view, we show representative spike raster diagrams of the individual trials in Fig. 8. By increasing the strength of the photocurrent, we hardly find changes among pyramidal cells. However, the PV+ cells switch to rhythmic spiking activity synchronously. All parameters set in the optogenetic stimulation protocols ensure to protect cells from breakdown. Hence, the optogenetic stimulation on PV+ cells only (with reasonable protocol settings) seem unsuccessful in inhibiting LVF-seizures.

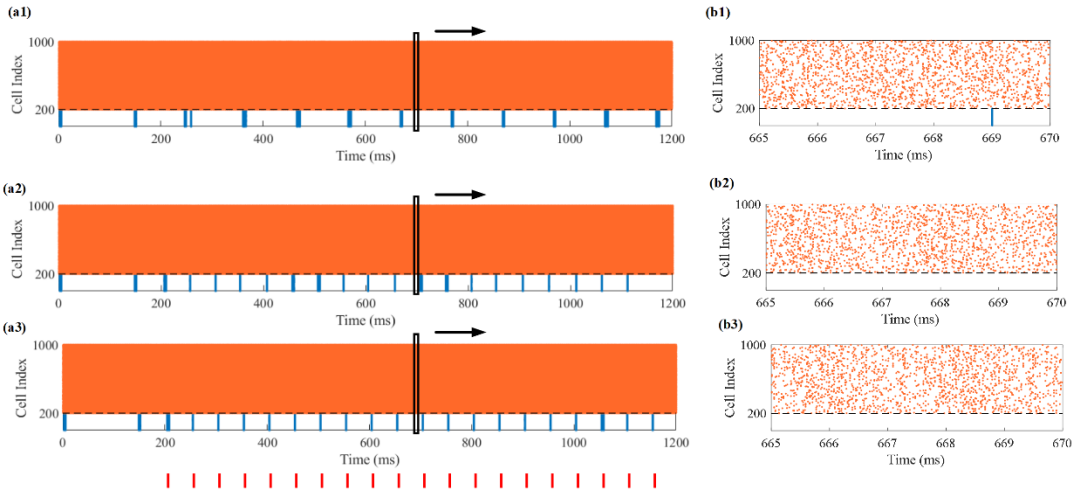

Figure 8. Spike raster diagrams of the hippocampal network under optogenetic stimulation on PV+ cells. The red rectangles indicate light pulses. (a1), (a2) and (a3) show situations where g_1 is equal to 10, 30 and 50 mS/cm^2, respectively. (b1), (b2) and (b3) plot detailed drawings from 665ms to 670ms. The spike raster diagram of the network where dark blue dots for index 1 to 200 represent spikes of PV+ cells and the orange dots are spikes of pyramidal cells.

Next, we test whether the optogenetic stimulation has effects on pyramidal cells. As the same stimulation protocols above, we change stimulation targets from PV+ cells to pyramidal cells. In the first trial Fig. 9(a1) and (b1)), both pyramidal cells and PV+ cells show little response to light pulses. Increasing the strength of the photocurrent (g_1 equals to 20 and 30 mS/cm^2, respectively), PV+ cells show some rhythmic bursts while the pyramidal cells remain unresponsive. Increasing g_1 to 40 mS/cm^2, both cells show distinct responses as soon as the photocurrent is injected. Pyramidal cells show large inhibitory postsynaptic potentials (IPSPs) when light pulses arrive, and then switch to rhythmic spiking in low frequency while PV+ cells transit to rhythmic spiking. Finally, if we change g_1 to 50 mS/cm^2, we obtain similar results to $g_1 = 40 mS/cm^2$. Spike raster diagrams of the three qualitatively different situations are shown in Fig. 10. These computational results provide evidence that optogenetic stimulation can successfully suppress LVF seizure-onset when photocurrent is injected to pyramidal cells.

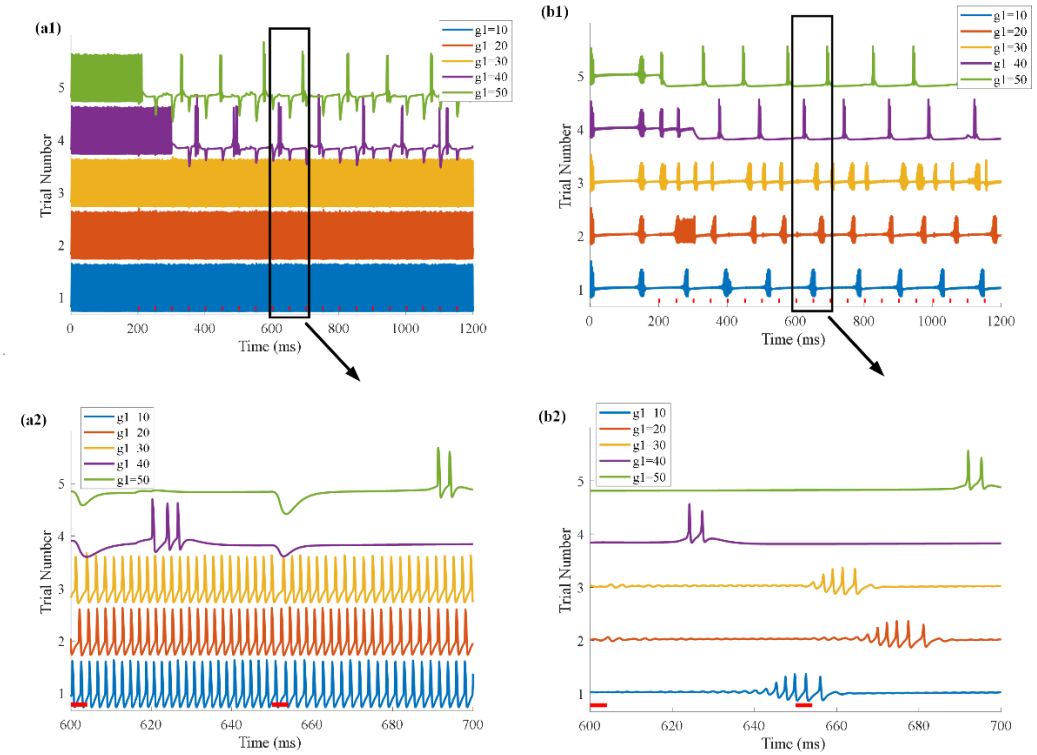

Figure 9. Time series of pyramidal cell and PV+ cell under optogenetic stimulation on pyramidal cells. The red rectangles denote light pulses. (a1) shows results (time plots in dark blue, dark orange, yellow, purple and green) of five trials for pyramidal cell corresponding to $g_1 = 10, 20, 30, 40$ and $50 mS/cm^2$ and (a2) records details from 600ms to 700 ms. (b1) and (b2) show the same for a PV+ cell.

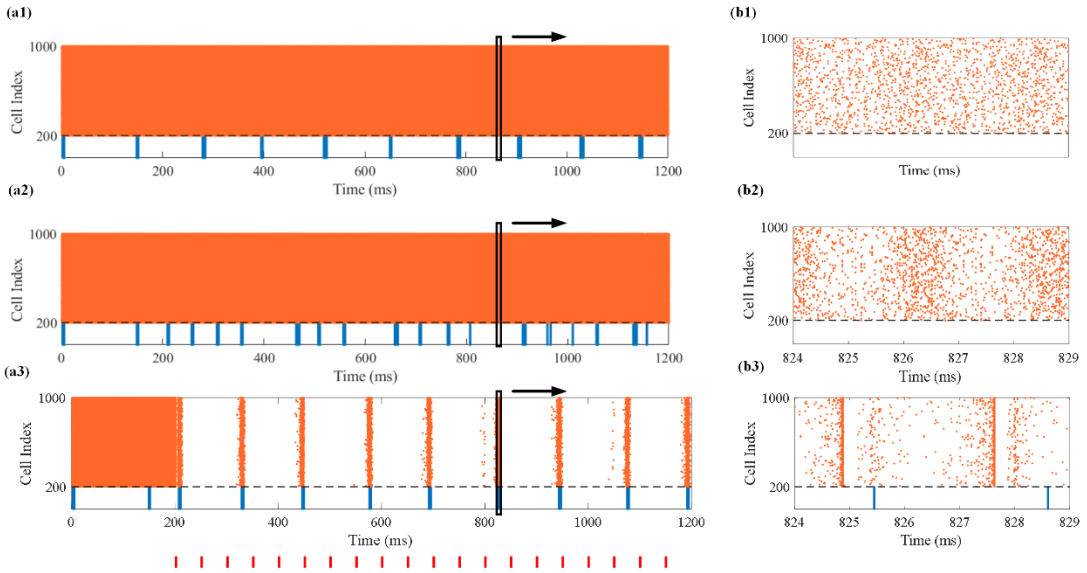

Figure 10. Spike raster diagrams of the hippocampal network under optogenetic stimulation on pyramidal cells. The red rectangles indicate light pulses. (a1), (a2) and (a3) show situations as g_1 equals to 10, 30 and 50 mS/cm^2, respectively. (b1), (b2) and (b3) show detailed drawings from 824ms to 829ms.

To further make comparisons between different optogenetic stimulation protocols driving pyramidal cells, we depict control effects from a dynamical point of view. The left panel in Fig. 11 illustrates the phase space consisting of membrane potential and activation variable of potassium ions (n) under small optogenetic stimulations ($g_1 = 10mS/cm^2$). The yellow star indicates the point when the photocurrent is injected. We can observe that trajectories of a pyramidal cell before and after stimulation follow the same limit cycle. The phase portrait of a pyramidal cell exhibiting a cyclic trajectory means that the neuronal system is in a continuously spiking state. A small perturbation cannot pull the oscillator to another state. The phase portrait of a PV+ cell shows a combination of regular small oscillations forming a tube-like structure and large loops of various sizes. There is also no qualitative transition of the dynamics under these small disturbances. The right panel in Fig. 11 is plotted when the network receives strong optogenetic stimulation ($g_1 = 50mS/cm^2$). Both the pyramidal cell and PV+ cell undergo a qualitative transition. The yellow star indicates the point when one attractor loses its stability and the system transits to another trajectory qualitatively different from the original one. Comparing Fig. 11 with Fig. 5, we also observe that the trajectories of the seizure state and the normal rhythmic oscillation are close to each other making it more likely that an appropriate perturbation induces a transition.

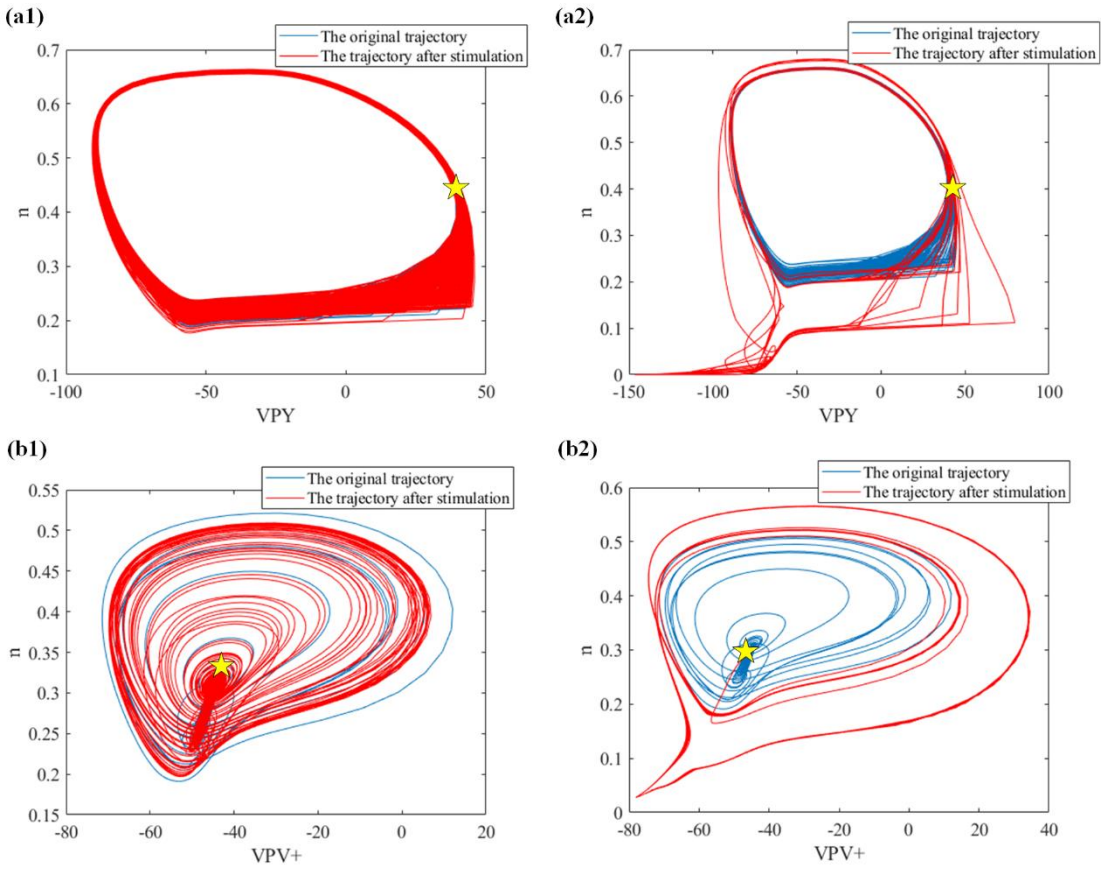

Figure 11. The phase state portraits with membrane potentials and activation variable of potassium ion under optogenetic stimulation. (a1) and (b1) are results with small perturbance ($g_1 = 10mS/cm^2$) for the pyramidal and PV+ cell, respectively. (a2) and (b2) are results of a strong perturbance ($g_1 = 50mS/cm^2$). The dark blue curves represent the original states, and the red curves indicate states after stimulations. The yellow pentagrams indicate the stimulation points.

Discussion & Conclusions

The activation of specific neuronal networks leads to different seizure-onset types in focal epilepsies (Shiri et al. 2016). In this work, we constructed a biophysical network to investigate the mechanisms underlying LVF seizure-onset in the hippocampus. The configuration of the neuronal network is based on experimental results. We use the pyramidal cell model of Olufsen et al. (2003). The pyramidal cells were modeled by the Hodgkin-Huxley type equations (Hodgkin and Huxley, 1952). Cells were given basic sodium and potassium spiking currents, a leak current, and a given external current density (Olufsen et al. 2003). For PV+ cell, we use the Wang and Buzsáki (1996) model. As in the pyramidal cell model, the spiking-generating sodium and potassium voltage-dependent ion currents of PV+ cell are of the Hodgkin-Huxley type. Different from the Hodgkin-

Huxley model, the Wang and Buzsáki model displays two salient properties of hippocampal and neocortical fast-spiking interneurons. One is that the action potential of PV+ cell is followed by a brief afterhyperpolarization, the other one is that the PV+ cell has the ability to fire repetitive spikes at high frequencies (Wang and Buzsáki, 1996). For the synaptic model, we adopt a model by Ermentrout and Kopell (1998). The model simulates AMPA and $GABA_A$ receptor-mediated synapses, respectively. The actual dynamics of the neuronal network depends on the patterns of synaptic connectivity. In computational modelling, connections are often made randomly with a fixed probability, i.e. an Erdös-Rényi (ER) model (Erdös and Rényi, 1959). According to the ER model, the network starts with N nodes and connects every pair of nodes with probability p, then creates a graph with approximately $\frac{pN(N-1)}{2}$ links distributed randomly (Albert and Barabási, 2002). However, studies suggest that the actual patterns of connectivity between neurons are quite different from the ER random network (Perin et al. 2011, Duane QN et al. 2017). Many studies of a range of anatomical parts of the brain and scales have found that networks may exhibit complex connectivity properties, which indicates they display inhomogeneous features characteristic of a combination of both regularity and randomness (Bullmore and Sporns 2009, Prettejohn et al 2011). In addition, many neuronal networks appear to be approximately scale-free, meaning that their node degrees follow a power-law distribution. Buzsáki et al. (Buzsáki et al 2004) pointed out that distinct classes of interneurons could drive connections having a different length scale, which enables global synchrony and oscillations. Therefore, we chose the scale-free topology to construct our biophysical network, rather than the ER structure. This cell assembly configuration guarantees the occurrence of gamma rhythm, and has the ability to reproduce the transition from gamma rhythm to epileptic oscillation and vice versa.

In the CA3 network model we found that influences from PV+ cells including the extracellular concentration of potassium ions and synaptic responses could induce LVF seizure-onset and fast spiking in the interneuron and the pyramidal cell population. This agrees with the observation that seizure-like events with an LVF onset pattern can be triggered by interneuronal network activity (Shiri et al. 2016). Cressman et al. (2009) showed that there is a broad range of potassium concentrations of a single neuron, especially values supporting stable periodic oscillations, which induce seizure-like behavior and match experimental phenomena well. As Cressman et al. point out,

if we continue to elevate the reservoir potassium concentration, the model will ultimately reach a new stable extracellular potassium concentration. In our study, we set the potassium conductance g_k within a reasonable range according to previous computational simulations, to maintain the intrinsic dynamical characteristics of individual cells. Furthermore, Depannemaecker et al. (2022) gradually increased the concentration of potassium which led to seven firing patterns, and the Nernst potentials showed a transient change, or an oscillation linked to periodic activities, which is related to ionic homeostatic regulation. They also indicated that the activity of the neuronal network could not be seen as a simple combination of seizures at the single neuron level because it included many complex nonlinear components. In terms of our research, we regulated the extracellular potassium concentration in a moderate range to drive the network to exhibit both normal oscillation and seizure-like behaviors. We then examined and compared the phase space trajectories of rhythmic oscillations and morbid activity. It is worth noting that the seizure attractor also exists even in the model of normal activity. However, in this case, the trajectories corresponding to seizure and normal dynamics are well separated which means random perturbations do not result in transitions between them. In the "epileptic" model, the trajectories lie closely together (Fig. 11), and proper perturbations produce transitions between the normal and the seizure state (Lytton 2008). In addition, we depicted the effects of PV+ cells on network dynamics quantificationally. Using extensive simulation work, we reproduced various dynamical activities including gamma rhythmic oscillation, fast spiking, LVF seizure-onset, etc. The parameter spaces shown in Fig. 6 provide a frequency-based guidance to explore the transition mechanisms.

In vitro and *in vivo* experiments have shown that GABAergic interneurons favor seizure initiation (Truccolo et al. 2011; Schevon et al. 2012; Grasse et al. 2013). Therefore, it is reasonable to take PV+ interneurons as the stimulation targets for suppressing seizures. Based on the advanced optogenetic techniques, we began to apply photocurrents to PV+ cells. Surprisingly, light protocols with various pulse strength did not terminate LVF seizure-onset. The impact of PV+ cells on seizure activity is not simple. A recent study by Lévesque and colleagues (Lévesque et al, 2022) showed that a type of bilateral optogenetic stimulation of PV+ interneurons in the CA3 region of the hippocampus during the chronic epileptic period does not induce anti-ictogenic effects; on the contrary, it facilitates and increases epileptiform excitability in hippocampal networks. This conclusion is in agreement with their earlier study (Lévesque, Chen et al, 2019): PV+ interneuron

stimulation can trigger seizures in epileptic animals, that is, $GABA_A$ signaling can also be ictogenetic. Assaf and Schiller (Assaf and Schiller, 2016) investigated the potential mechanism of PV+ cells on ictogenesis, finding synchronized post-inhibition rebound firing of pyramidal neurons. It is also reported that optogenetic activation of PV+ interneurons triggers LVF seizure-onset by using enhanced ChR2 opsin (Shiri et al. 2015). These results may explain why the PV+ cell-driven optogenetic control is unsuccessful in our model. We therefore switched to the pyramidal cells as targets. In this case, the network dynamics of CA3 transits from the morbid state to normal rhythmic oscillations as soon as appropriate photocurrents are injected. These findings also indicate a shortcoming of a control strategy based the network topology alone, i.e., hub neurons may not necessarily be the ideal targets.

Using our model, the dynamic mechanism of the most common type of focal seizure-onset in adult temporal lobe epilepsy and its response to optogenetic stimulation can be explored. The limitations of our research are that 1) transitions between and among different types of seizure-onset didn't appear in this network; and 2) the results may be depended on the network structure to some extent. We will need to modify the present network structure and produce multiple states to enrich our knowledge about dynamics of different types of seizure-onset and their response to stimulation. Furthermore, more advanced control theory could be added to assist the optogenetic perturbation strategy to get improved results. We hope that such computational work will provide a theoretical basis for clinical research and treatment drug-resistant epilepsy.

Acknowledgements

This work was supported by the National Key Research and Development Program of China (Grant Nos. 2021YFA1000200 and 2021YFA1000202), the National Natural Science Foundation of China (Grant Nos. 12102014 and 11932003), the China Postdoctoral Science Foundation (Grant No. 2021M700307), and the Beijing Postdoctoral Research Foundation (Grant No.2021-ZZ-058).

Author Contributions

YL and GB contributed equally to this work. LZ, ZM, YY, BL, SW, YL and GB designed ideas, performed algorithm implementation, analyzed the data, and wrote the paper. All authors contributed to the article.

Data Availability

The data that support the findings of this study are available from the corresponding author upon reasonable request.

Declarations

Conflict of interest: The authors declare that the research was conducted in the absence of any commercial or financial relationships that could be construed as a potential conflict of interest.

References

Albert R and Barabási A (2002) Statistical mechanics of complex networks. Reviews of Modern physics, 74(1): 47-97. http://doi.org/10.1103/RevModPhys.74.47

Assaf F and Schiller Y (2016) The antiepileptic and ictogenic effects of optogenetic neurostimulation of PV-expressing interneurons. Journal of Neurophysiology, 116(4):1694-1704. https://doi.org/10.1152/jn.00744.2015

Avoli M and de Curtis M (2011) GABAergic synchronization in the limbic system and its role in the generation of epileptiform activity. Progress in Neurobiology, 95(2):104-132. http://doi.org/ 10.1016/j.pneurobio.2011.07.003

Avoli M, de Curtis M, Gnatkovsky V, et al (2016) Specific imbalance of excitatory/inhibitory signaling establishes seizure onset pattern in temporal lobe epilepsy. Journal of Neurophysiology, 115:3229-3237. http://doi.org/10.1152/jn.01128.2015

Barabási AL (2009) Scale-free network: a decade and beyond. Science, 325(5939):412-413. https://doi.org/10.1126/science.1173299

Barabási AL and Albert R (1999) Emergence of scaling in random networks. Science, 286(5439):509-512. https://doi.org/10.1126/science.286.5439.509

Bartos M, Vida I and Jonas P (2007) Synaptic mechanisms of synchronized gamma oscillations in inhibitory interneuron networks. Nature Reviews, 8:45-56. https://doi.org/10.1038/nrn2044

Bonifazi P, Goldin M, Picardo MA, et al (2009) GABAergic hub neurons orchestrate synchrony in developing hippocampal networks. Science, 326:1419. http://dx.doi.org/10.1126/science.1175509

Börgers C and Kopell N (2003) Synchronization in networks of excitatory and inhibitory neurons with sparse, random connectivity. Neural Computation, 15(3):509-538. https://doi.org/10.1162/089976603321192059

Boyden ES, Zhang F, Bamberg E, et al (2005) Millisecond-timescale, genetically targeted optical control of neural activity. Nature Neuroscience, 8(9):1263-1268. http://dx.doi.org/ 10.1038/nn1525

Bullmore E and Sporns O (2009) Complex brain networks: graph theoretical analysis of structural and functional systems. Nature Review Neuroscience, 10:186-198. http://doi.org/10.1038/nrn2575

Buzsáki G, Geisler C, Henze DA, et al (2004) Interneuron diversity series: circuit complexity and axon wiring economy of cortical interneurons. Trends in Neurosciences, 27(4):186-193. http://doi.org/ 10.1016/j.tins.2004.02.007

Cressman JR, Ullah G, Ziburkus J, et al (2009). The influence of sodium and potassium dynamics on excitability seizures, and the stability of persistent states: I. Single neuron dynamics. Journal of Computational Neuroscience, 26(2):159-170. https://doi.org/ 0.1007/s10827-008-0132-4

De Curtis M and Avoli M (2016) GABAergic networks jump-start focal seizures. Epilepsia, 57(5):679-687. http://doi.org/10.1111/epi.13370

Demont-Guignard S, Benquet P, Gerber U, et al (2012) Distinct hyperexcitability mechanisms underlie fast ripples and epileptic spikes. Annals of Neurology, 71(3):342-352. https://doi.org/10.1002/ana.22610

Depannemaecker D, Lvanov A, Lillo D, et al (2022). A unified physiological framework of transitions between seizures, sustained ictal activity and depolarization block at the single neuron level. Journal of Computational Neuroscience, 50(1):33-49. https://doi.org/10.1007/s10827-022-00811-1

Du M, Li J, Wang R, et al (2016) The influence of potassium concentration on epileptic seizures in a coupled neuronal model in the hippocampus. Cognitive Neurodynamics, 10:405-414. http://dx.doi.org/10.1007/s11571-016-9390-4

Duane QN, Daniel F, Sammy S et al (2017) Mean-field equations for neuronal networks with arbitrary degree distributions. Physical Review E, 95:042323. http://doi.org/10.1103/PhysRevE.95.042323

Dugladze T, Maziashvili N, Borgers C, et al (2013) GABA(B) autoreceptor-mediated cell type-specific reduction of inhibition in epileptic mice. Proceedings of the National Academy of Sciences of the United States of America, 110(37):15073-15078. https://doi.org/10.1073/pnas.1313505110

Emerson J, Afelin A, Sliupas V, et al (2019) Identifying influential nodes in a network model of epilepsy. Journal of Nonlinear Science, 30:2283-2308. https://doi.org/10.1007/s00332-019-09545-4

Engel J, Bragin A, Staba R, et al (2009). High-frequency oscillations: what is normal and what is not? Epilepsia, 50(4):598-604. https://doi.org/10.1111/j.1528-1167.2008.01917.x

Erdös P and Rényi A (1959) On Random Graphs. I. Publicationes Mathematicae 6: 290–297. http://doi.org/10.1109/ICSMC.2006.384625

Ermentrout GB and Kopell N (1998) Fine structure of neural spiking and synchronization in the presence of conduction delay. Proceedings of the National Academy of Sciences of the United States of America, 95(3):1259-1264. https://doi.org/10.1073/pnas.95.3.1259

Evangelista R, Cano G, Copper C, et al (2020) Generation of sharp wave-ripple events by disinhibition/ The Journal of Neuroscience, 40(41):7811-7836. https://doi.org/10.1523/JNEUROSCI.2174-19.2020

Ferguson KA, Chatzikalymniou AP, and Skinner FK (2017) Combining theory, model, and experiment to explain how intrinsic theta rhythms are generated in an in vitro whole hippocampus preparation without oscillatory inputs. eNeuro, 4(4): e0131-17.2017. http://dx.doi.org/10.1523/ENEURO.0131-17.2017

Foutz TJ, Arlow RL and McIntyre CC (2012) Theoretical principles underlying optical stimulation of a channelrhodopsin-2 positive pyramidal neuron. Journal of Neurophysiology, 107:3235-3245. https://doi.org/10.1152/jn.00501.2011

Franaszczuk PJ, Kudela P and Bergey GK (2003). External excitatory stimuli can terminate bursting in neural network models. Epilepsy Research, 53(1-2):65-80. https://doi.org/10.1016/S0920-1211(02)00248-6

Gadhoumi K, Gotman J and Lina JM (2015) Scale invariance properties of intracerebral EEG improve seizure prediction in mesial temporal lobe epilepsy. PLoS ONE, 10(4):e0121182. https://doi.org/10.1371/journal.pone.0121182

Gafurov B and Bausch SB (2013) GABAergic transmission facilitates ictogenesis and synchrony

between CA3, hilus, and dentate gyrus in slices from epileptic rates. Journal of neurophysiology, 110(2):441-455. https://doi.org/10.1152/jn.00679.2012

Grasse DW, Karunakaran S and Moxon KA (2013) Neuronal synchrony and the transition to spontaneous seizures. Experimental Neurology, 248:72-84. https://doi.org/10.1016/j.expneurol.2013.05.004

Hodgkin AL and Huxley AF (1952) Currents carried by sodium and potassium ions through the membrane of the giant axon of loligo. The Journal of Physiology, 116(4):449-472. https://doi.org/10.1113/jphysiol.1952.sp004717

Howe T, Blockeel AJ, Taylor H, et al (2020) NMDA receptors promote hippocampal sharp-wave ripples and the associated coactivity of CA1 pyramidal cells. Hippocampus, 30:1356-1370. https://doi.org/10.1002/hipo.23276

Jiruska P, de Curtis M, Jefferys JGR, et al (2013) Synchronization and desynchronization in epilepsy: controversies and hypotheses. The Journal of Physiology, 591(4):787-797. https://doi.org/10.1113/jphysiol.2012.239590

Kopell N, Börgers C, Pervouchine D, et al (2010) Gamma and theta rhythms in biophysical models of hippocampal circuits. In: Cutsuridis V, Graham B, Cobb S, et al. (eds) Hippocampal Microcircuits. Springer Series in Computational Neuroscience, vol 5. Springer, New York, pp 423-457. https://doi.org/10.1007/978-1-4419-0996-1_15

Krook-Magnuson E and Soltesz I (2015) Beyond the hammer and the scalpel: selective circuit control for the epilepsies. Nature Neuroscience, 18(3):331-338. https://doi.org/10.1038/nn.3943

Krook-Magnuson E, Armstrong C, Oijala M, et al (2013) On-demand optogenetic control of spontaneous seizures in temporal lobe epilepsy. Nature Communication, 4:1376. http://dx.doi.org/10.1038/ncomms2376

Krook-Magnuson E, Szabo GG, Armstrong C, et al (2014) Cerebellar directed optogenetic intervention inhibits spontaneous hippocampal seizures in a mouse model of temporal lobe epilepsy. eNeuro, 1(1):e.2014. http://dx.doi.org/10.1523/ENEURO.0005-14.2014

Lee SA, Spencer DD and Spencer SS (2000) Intracranial EEG seizure-onset patterns in neocortical epilepsy. Epilepsia, 41(3):297-307. http://doi.org/10.1111/j.1528-1157.2000.tb00159.x

Lévesque M and Avoli M (2019) High-frequency oscillations and focal seizures in epileptic rodents. Neurobiology of Disease, 124:396-407. https://doi.org/10.1016/j.nbd.2018.12.016

Lévesque M, Chen L, Etter G, et al (2019) Paradoxical effects of optogenetic stimulation in mesial temporal lobe epilepsy. Annals of Neurology, 86(5):714-728.

Lévesque M, Salami P, Gotman J, et al (2012) Two seizure-onset types reveal specific patterns of high-frequency oscillations in a model of temporal lobe epilepsy. The Journal of Neuroscience, 32(38):13264-13272. https://doi.org/10.1523/JNEUROSCI.5086-11.2012

Lévesque M, Shiri Z, Chen LY, et al (2018) High-frequency oscillations and mesial temporal lobe epilepsy. Neuroscience Letters, 667:66-74. https://doi.org/10.1016/j.neulet.2017.01.047

Lévesque M, Wang S, Etter G, et al (2022) Bilateral optogenetic activation of inhibitory cells favors ictogenesis. Neurobiology of Disease, 171:105794. https://doi.org/10.1016/j.nbd.2022.105794

Lytton WW (2008) Computer modelling of epilepsy. Nature Reviews Neuroscience, 9(8):626-637. https://doi.org/10.1038/nrn2416

Marafiga JR, Pasquetti MV and Calcagnotto ME (2021) In vitro oscillation patterns throughout the hippocampal formation in a rodent model of epilepsy. Neuroscience, 479:1-21. https://doi.org/10.1016/j.neuroscience.2021.10.020

Mushtaq M, ul Haq R, Anwar W, et al (2021) A computational study of suppression of sharp wave ripple complexes by controlling calcium and gap junctions in pyramidal cells. Bioengineered, 12(1):2603-2651. https://doi.org/10.1080/21655979.2021.1936894

Nagel G, Szellas T, Huhh W, et al (2003) Channelrhodopsin-2, a directly light-gated cation-selective membrane channel. Proceedings of the National Academy of Sciences of the United States of America, 100(24):13940-13945. https://doi.org/10.1073/pnas.1936192100

Nikolic K, Grossman N, Grubb MS, et al (2009) Photocycles of channelrhodopsin-2. Photochemistry and Photobiology, 85:400-411. https://doi.org/10.1111/j.1751-1097.2008.00460.x

Olteanu C, Habibollahi F and French C (2021) Effects of several classes of voltage-gated ion channel conductances on gamma and theta oscillations in a hippocampal microcircuit model. Frontiers in computational neuroscience, 15:630271. http://dx.doi.org/10.3389/fncom.2021.630271

Olufsen M, Whittington M, Camperi M, et al (2003) New functions for the gamma rhythm: population tuning and preprocessing for the beta rhythm. Journal of Computational Neuroscience, 14(1):33-54. https://doi.org/10.1023/a:1021124317706

Olufsen M, Whittington M, Camperi M, et al (2003) New functions for the gamma rhythm: population tuning and preprocessing for the beta rhythm. Journal of Computational Neuroscience, 14(1):33-54. https://doi.org/10.1023/a:1021124317706

Oprisan SA, Buhusi M and Buhusi CV (2018) A population-based model of the temporal memory in the hippocampus. Frontiers in computational neuroscience, 12:521. http://dx.doi.org/10.3389/fnins.2018.00521

Pelliccia V, Mai R, Francione S, et al (2013) Ictal EEG modifications in temporal lobe epilepsy. Epileptic Disord, 15(4):392-399. http://doi.org/10.1684/epd.2013.0615

Perin R, Berger TK and Markram H (2011) A synaptic organizing principle for cortical neuronal groups. Proceedings of the National Academy of Sciences of the United States of America, 108(13):5419-5424. http://doi.org/ 10.1073/pnas.1016051108

Picardo MA, Guigue P, Bonifazi P, et al (2011) Pioneer GABA cells comprise a subpopulation of hub neurons in the developing hippocampus. Neuron, 71(4):695-709. http://dx.doi.org/10.1016/j.neuron.2011.06.018.

Prettejohn BJ, Berryman MJ and McDonnell MD (2011) Methods for generating complex networks with selected structural properties for simulations: a review and tutorial for neuroscientists. Frontiers in Computational Neuroscience, 5:11. http://doi.org/10.3389/fncom.2011.00011

Renault V, Thieullen M and Trélat E (2018) Minimal time spiking in various ChR-2-controlled neuron models. Journal of Mathematical Biology, 76(3):567-608. https://doi.org/10.1007/s00285-017-1101-1

Rezvani-Ardakani S, Mohammad-Ali-Nezhad S and Ghasemi R (2020) Epilepsy control using a fixed time integral super twisting sliding mode control for Pinsky–Rinzel pyramidal model through ion channels with optogenetic method. Computer Methods and Programs in Biomedicine, 195:105665. https://doi.org/10.1016/j.cmpb.2020.105665

Saggio ML, Crisp D, Scott JM, et al (2020) A taxonomy of seizure dynamotypes. eLife, 9:e55632. https://doi.org/10.7554/eLife.55632

Schevon CA, Weiss SA, McKhann G, et al (2012) Evidence of an inhibitory restraint of seizure activity in humans. Nature Communications, 3:1060. https://doi.org/10.1038/ncomms2056

Segneri M, Bi H, Olmi S, et al (2020) Theta-nested gamma oscillations in next generation neural mass models. Frontiers in Computational Neuroscience, 14:47. https://doi.org/10.3389/fncom.2020.00047

Shen Z, Zhang H, Cao Z, et al (2022) Transition dynamics and optogenetic controls of generalized periodic epileptiform discharges. Neural Networks, 149:1-17. https://doi.org/10.1016/j.neunet.2022.01.022

Shiri Z, Manseau F, Lévesque M, et al (2015) Interneuron activity leads to initiation of low-voltage fast-onset seizures. Annals of Neurology, 77(3):541-546. http://doi.org/10.1002/ana.24342

Shiri Z, Manseau F, Lévesque M, et al (2016) Activation of specific neuronal networks leads to different seizure onset types. Annals of Neurology79(3):354-365. https://doi.org/10.1002/ana.24570

Stam CJ and Reijneveld JC (2007) Graph theoretical analysis of complex networks in the brain. Nonlinear Biomedical Physics, 1(1):3. https://doi.org/10.1186/1753-4631-1-3

Stefanescu RA, Shivakeshavan RG, Khargonekar PP, et al (2013) Computational modeling of channelrhodopsin-2 photocurrent characteristics in relation to neural signaling. Bulletin of Mathematical Biology, 75(11):2208-2240. https://doi.org/10.1007/s11538-013-9888-4

Talathi SS, Carney PR and Khargonekar PP (2010) Control of neural synchrony using channelrhodopsin-2: a computational study. Journal of Computational Neuroscience, 31(1):87-103. https://doi.org/10.1007/s10827-010-0296-6

Taxidis J, Mizuseki K, Mason R, et al (2013) Influence of slow oscillation on hippocampal activity and ripples through cortico-hippocampal synaptic interactions, analyzed by a cortical-CA3-CA1 network model. Frontiers in Computational Neuroscience, 7:3. https://doi.org/10.3389/fncom.2013.00003

Tiesinga PHE (2012). Motifs in health and disease: the promise of circuit interrogation by optogenetics. European Journal of Neuroscience, 36(2):2260-2272. https://doi.org/10.1111/j.1460-9568.2012.08186.x

Tønnesen J, Sørensen AT, Deisseroth K, et al (2009) Optogenetic control of epileptiform activity. PNAS, 106(29):12162-12167. http://dx.doi.org/10.1073_pnas.0901915106

Truccolo W, Donoghue JA, Hochberg LR, et al (2011) Single-neuron dynamics in human focal epilepsy. Nature Neuroscience, 14(5):635-641. https://doi.org/10.1038/nn.2782

Wang X and Buzśaki G (1996) Gamma oscillation by synaptic inhibition in a hippocampal interneuronal network model. The Journal of Neuroscience, 16(20):6402-6413. https://doi.org/10.1523/JNEUROSCI.16-20-06402.1996

Wang X and Buzśaki G (1996) Gamma oscillation by synaptic inhibition in a hippocampal interneuronal network model. The Journal of Neuroscience, 16(20):6402-6413. https://doi.org/10.1523/JNEUROSCI.16-20-06402.1996

Yu Y, Han F, Wang Q, et al (2021) Model-based optogenetic stimulation to regulate beta oscillations in parkinsonian neural networks. Cognitive Neurodynamics. https://doi.org/10.1007/s11571-021-09729-3

Zhang H, Yu Y, D Z, et al (2020) Activity pattern analysis of subthalamopallidal network under channelRhodopsin-2 and halorhodopsin photocurrent control. Chaos, Solitons and Fractals, 138:109963. https://doi.org/10.1016/j.chaos.2020.109963

Zhang L, Wang Q and Baier G (2020) Dynamical features of a focal epileptogenic network model for stimulation-based control. IEEE Transactions on Neural Systems and Rehabilitation Engineering, 28(8):1856-1865. https://doi.org/10.1109/TNSRE.2020.3002350

Zhang L, Wang Q and Baier G (2020) Spontaneous transitions to focal-onset epileptic seizures: a dynamical study. Chaos, 30:103114. https://doi.org/10.1063/5.0021693

Figure 1(a)

Click here to access/download;Figure;Figure 1(a).tif

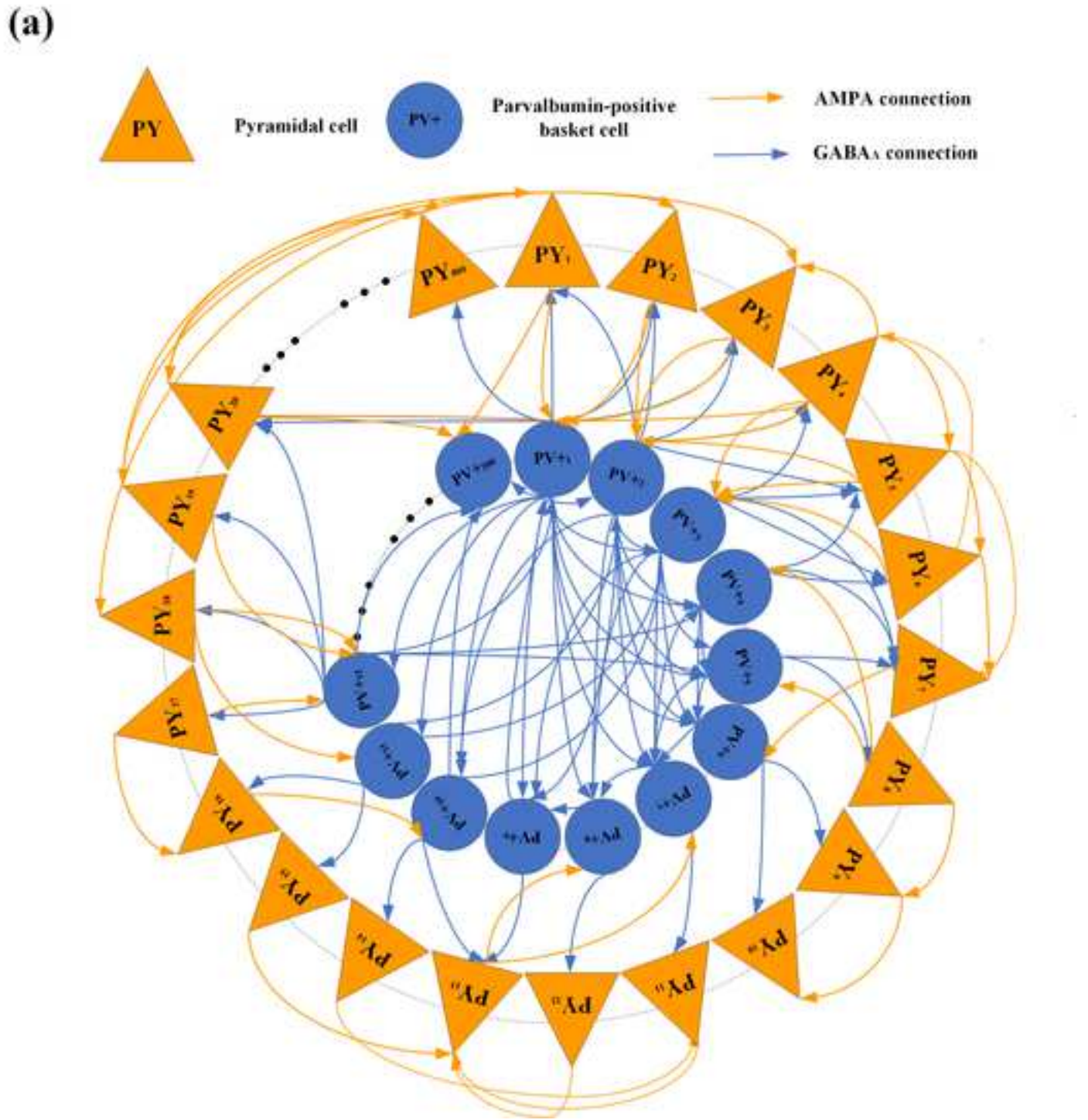

Figure 1(b)

Click here to access/download;Figure;Figure 1(b).tif

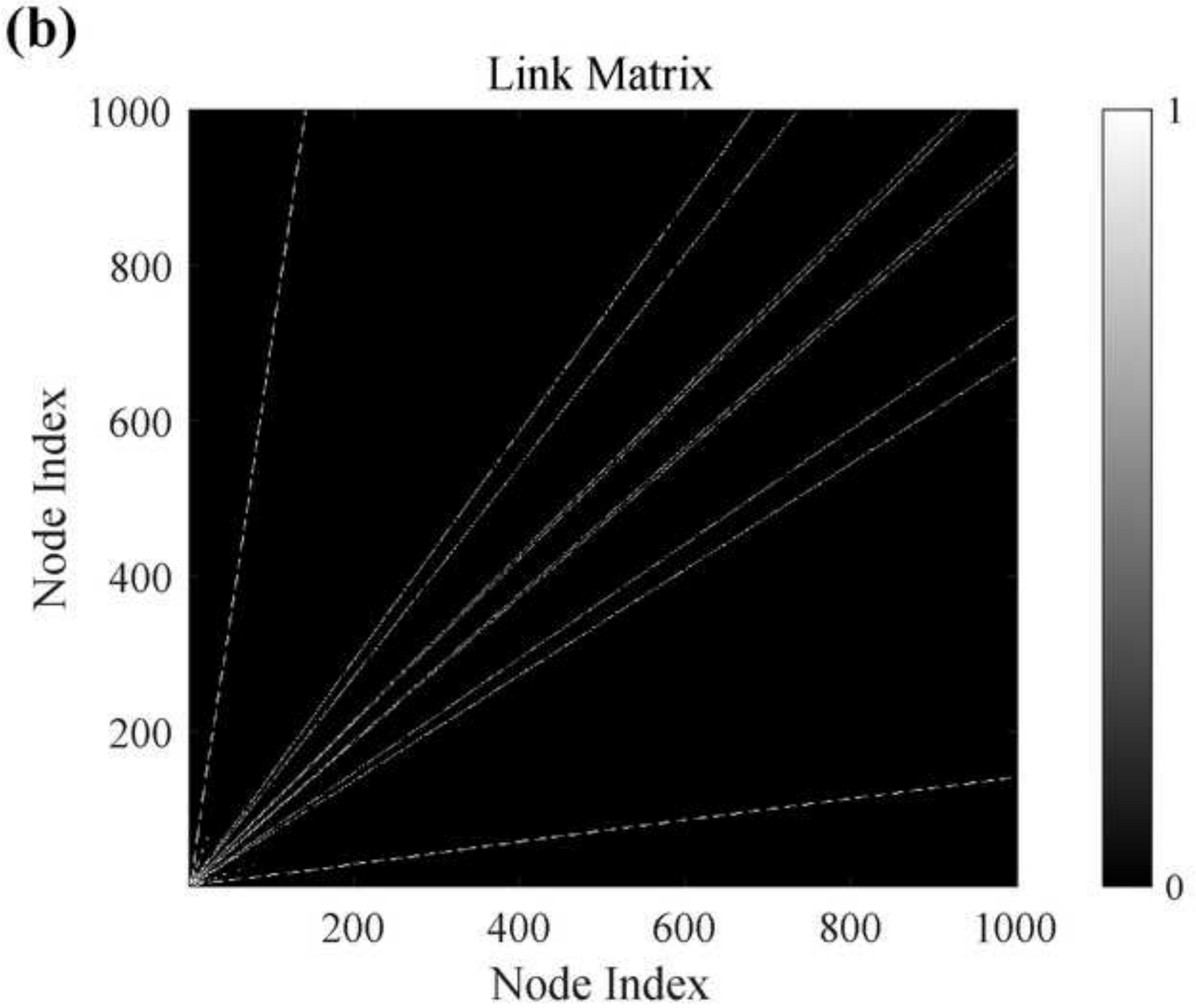

Figure 2(a)

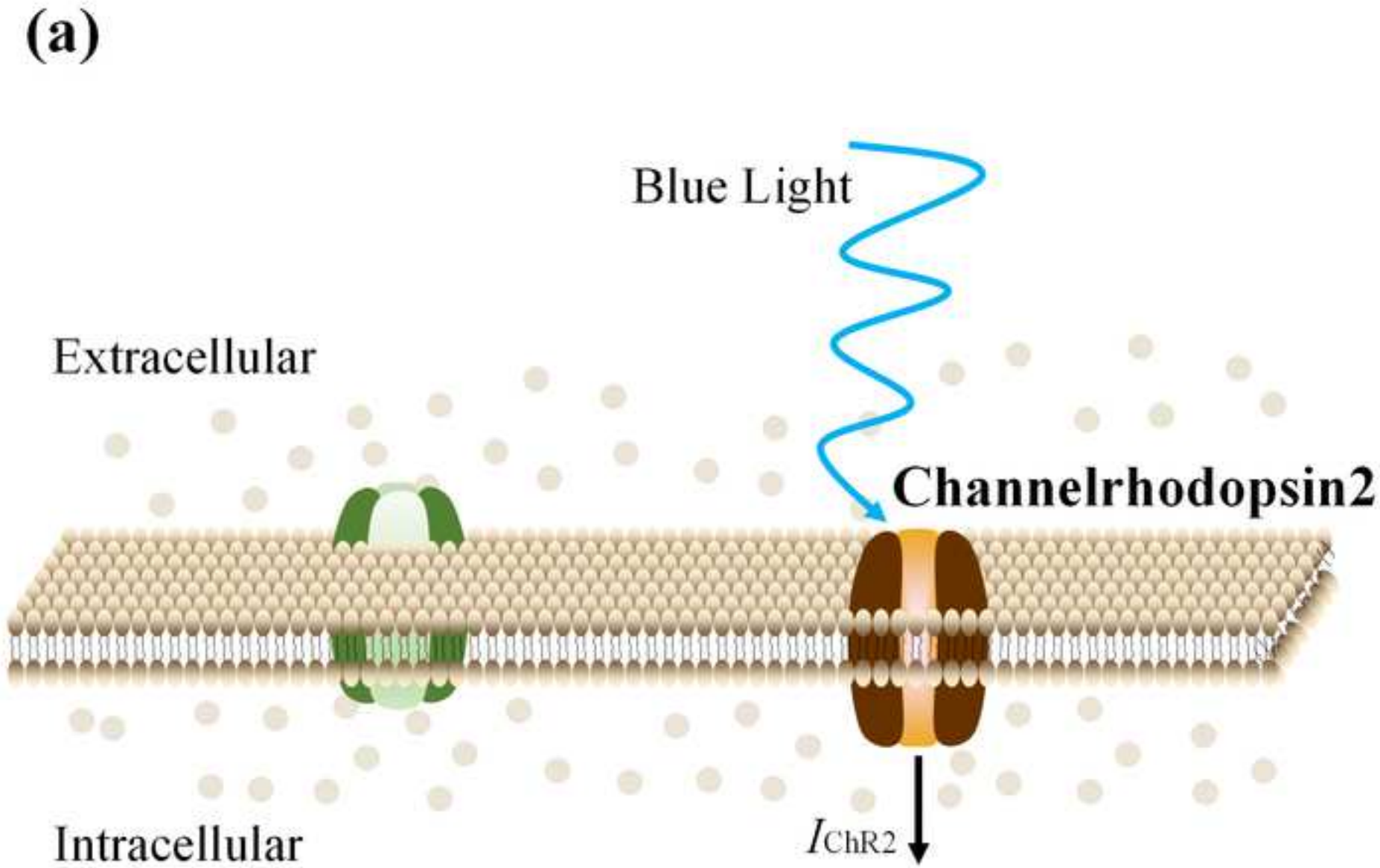

Figure 2(b)

Click here to access/download;Figure;Figure 2(b).tif

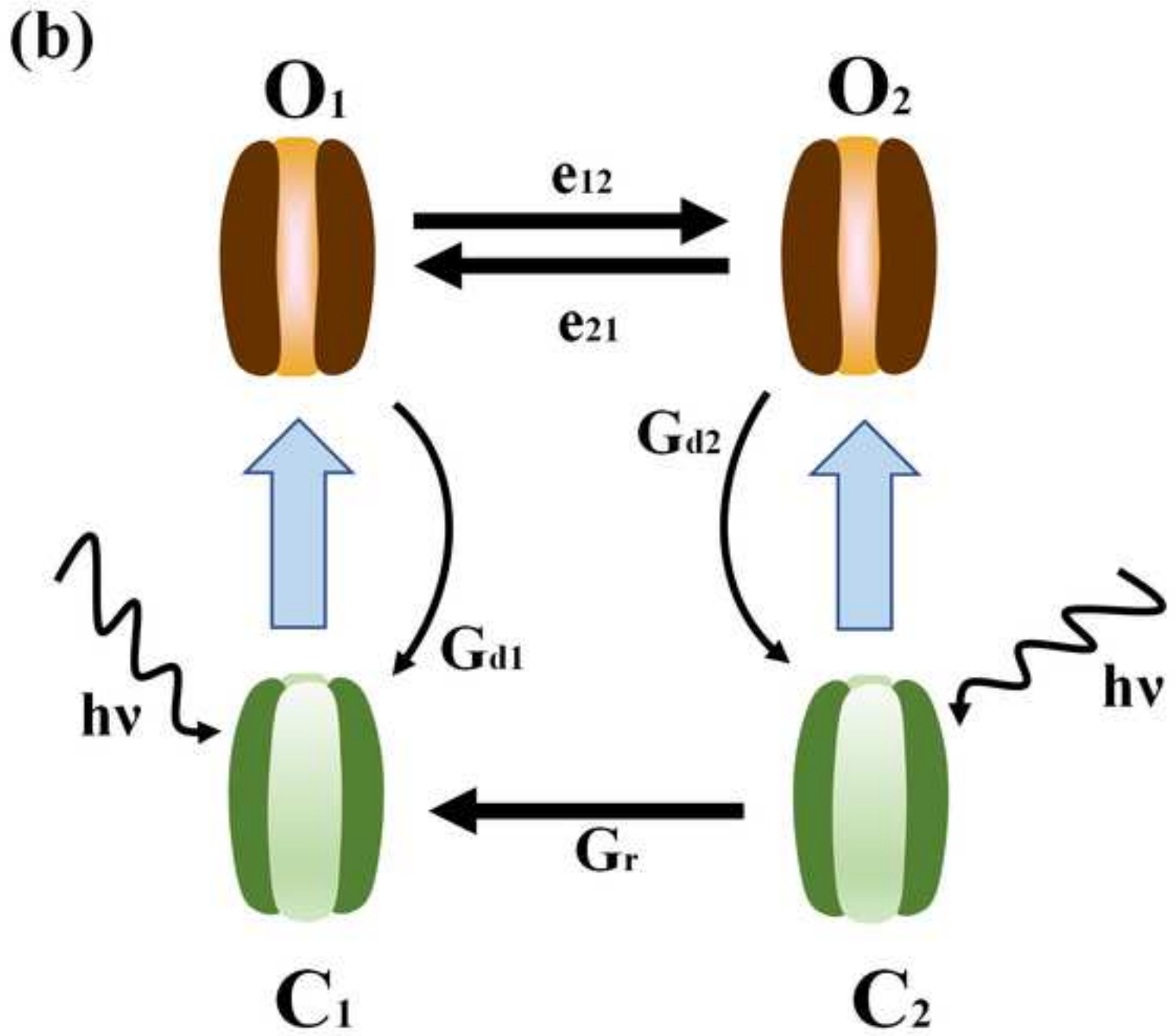

Figure 3

Click here to access/download;Figure;Figure 3.tif

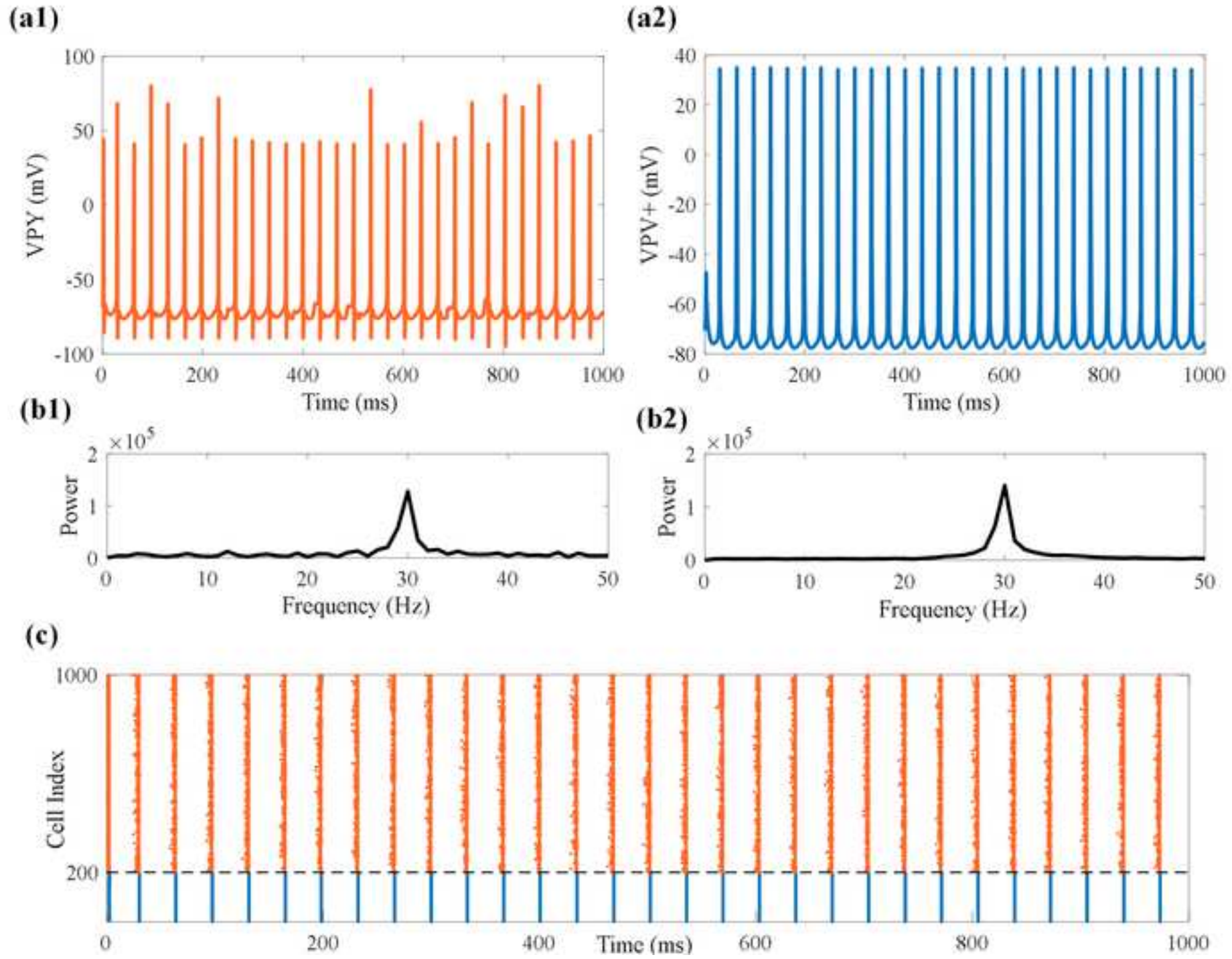

Figure 4

Click here to access/download;Figure;Figure 4.tif

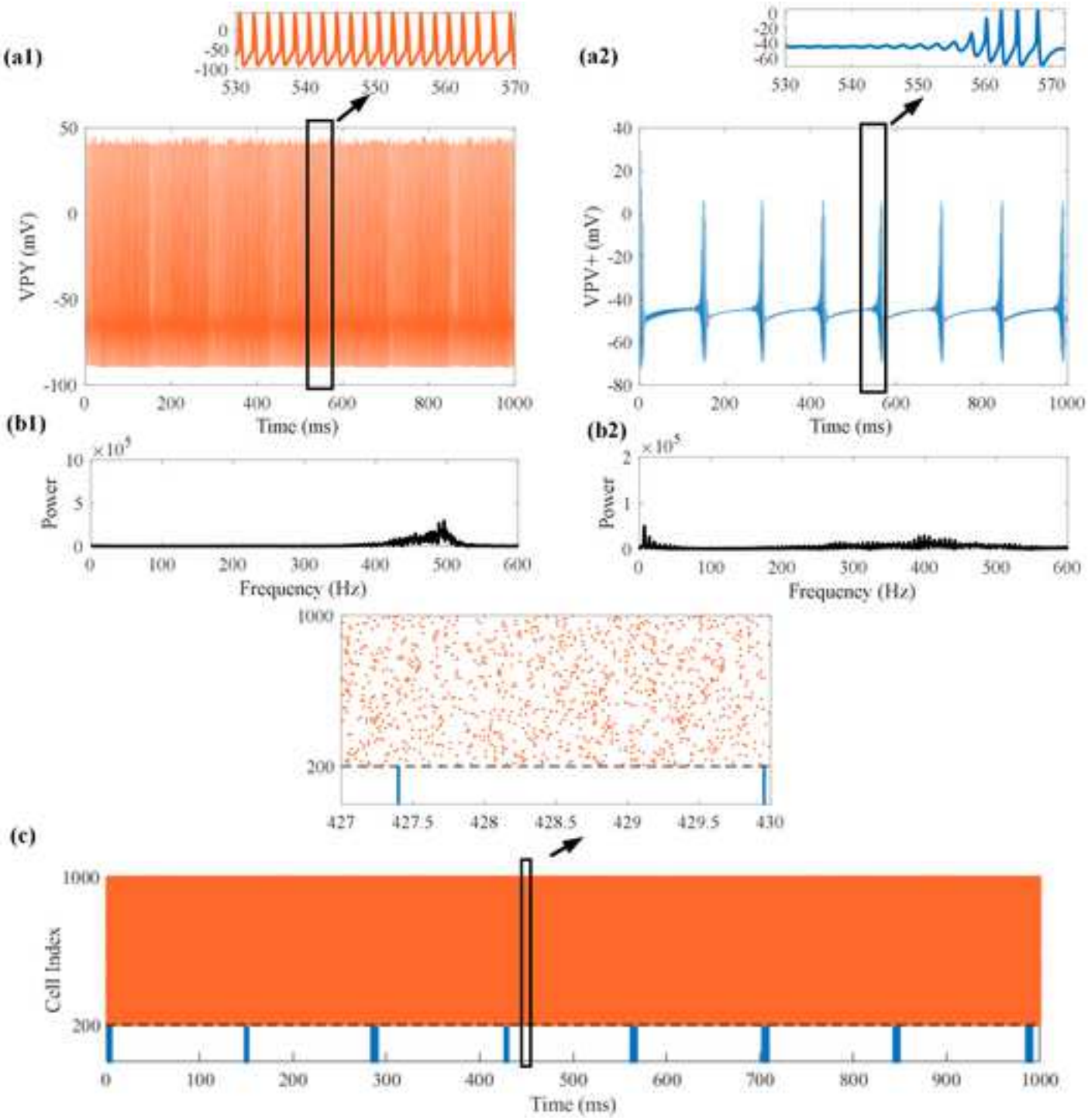

Figure 5(a1)(b1)

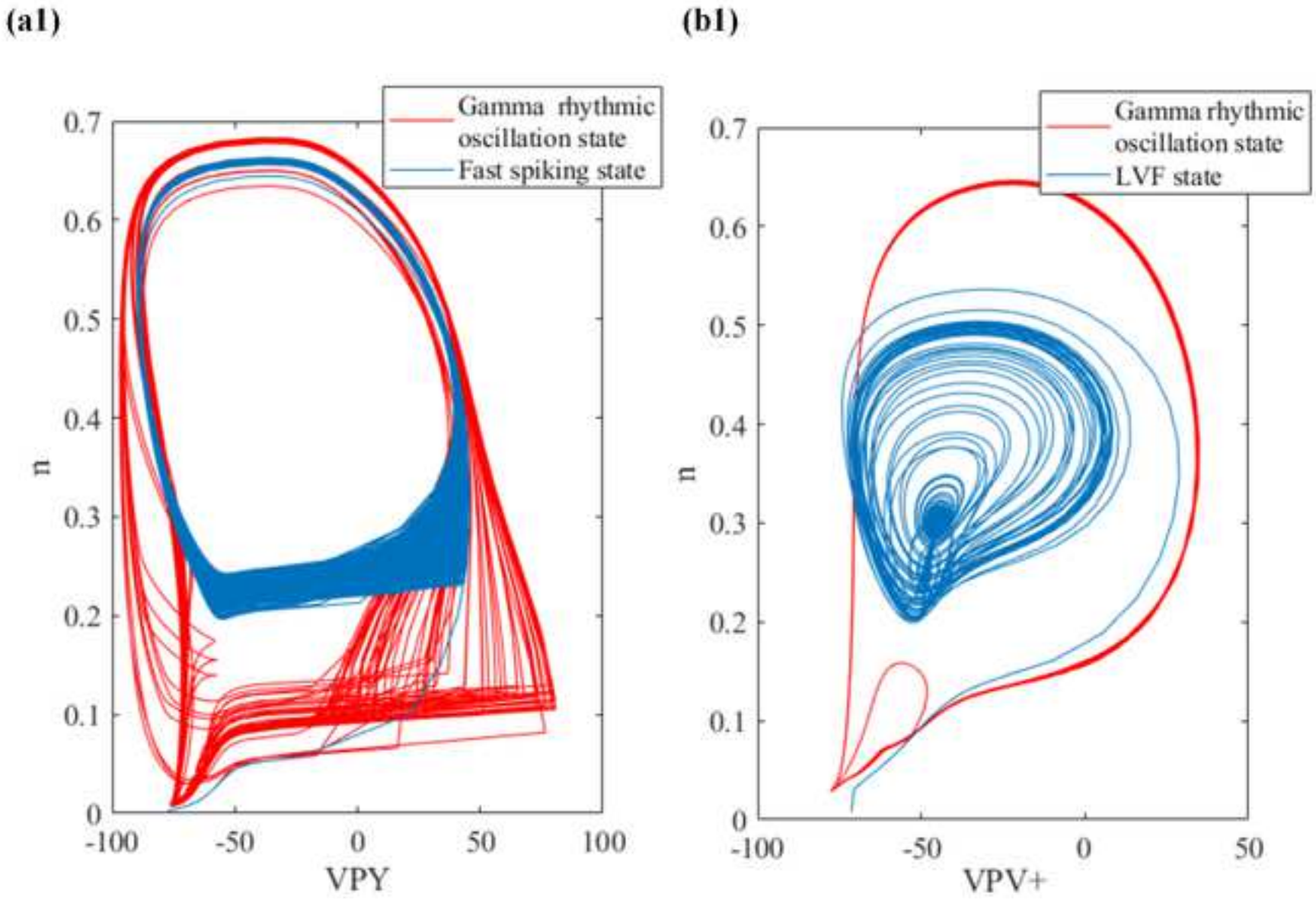

Figure 5(a2)(b2)

Click here to access/download;Figure;Figure 5(a2)(b2).tif

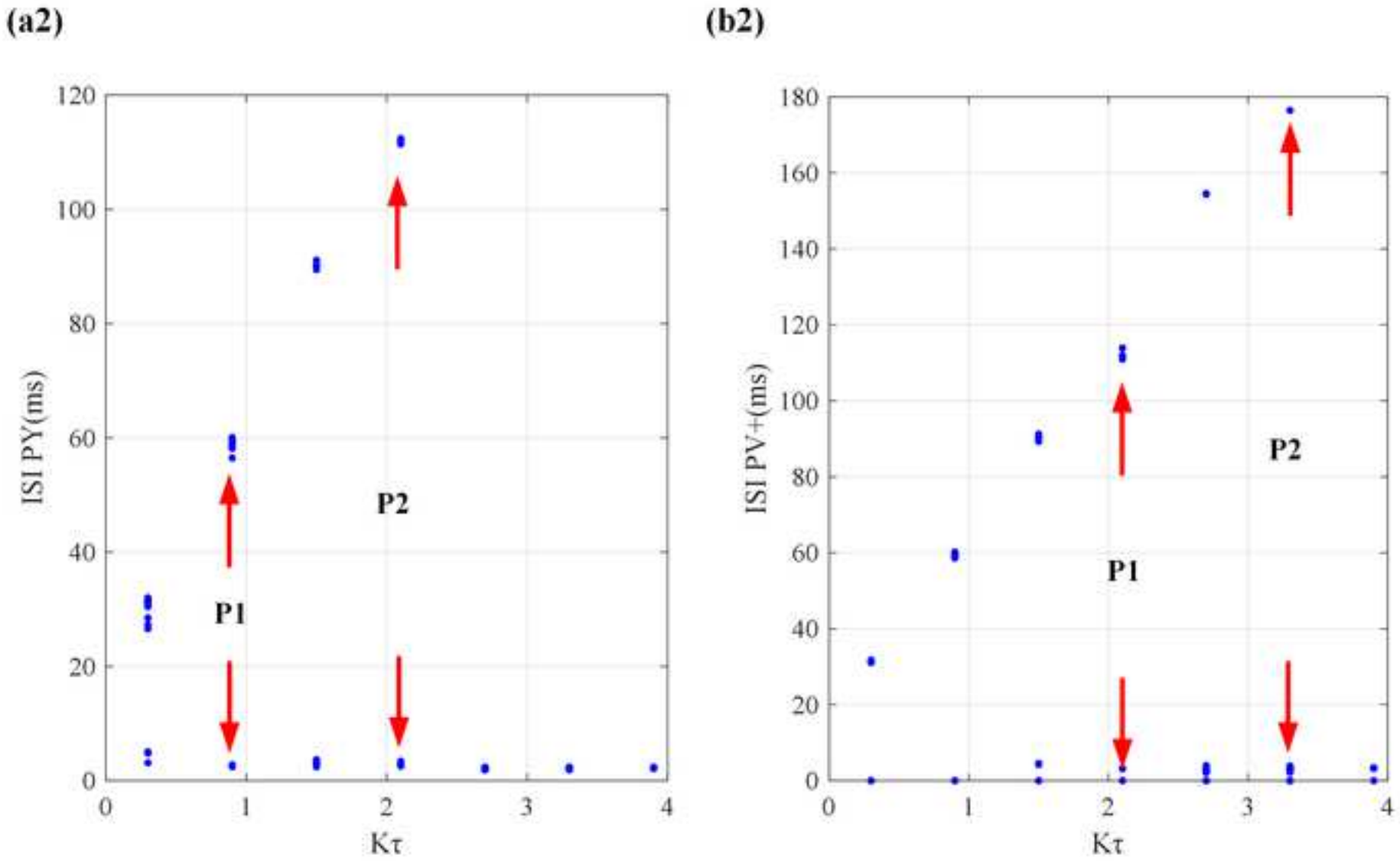

Figure 6(a1)(a2)

Click here to access/download;Figure;Figure 6(a1)(a2).tif

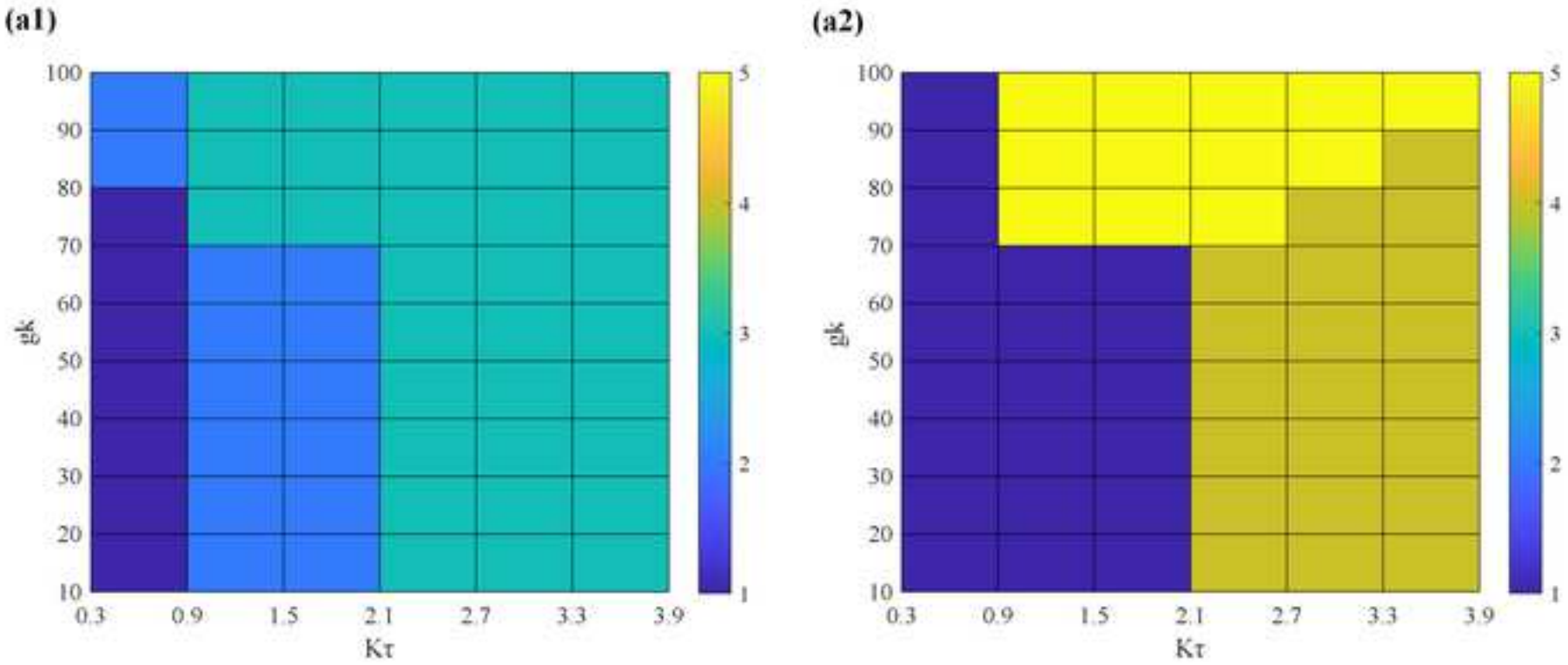

Figure 6(b1)(b2)

Click here to access/download;Figure;Figure 6(b1)(b2).tif

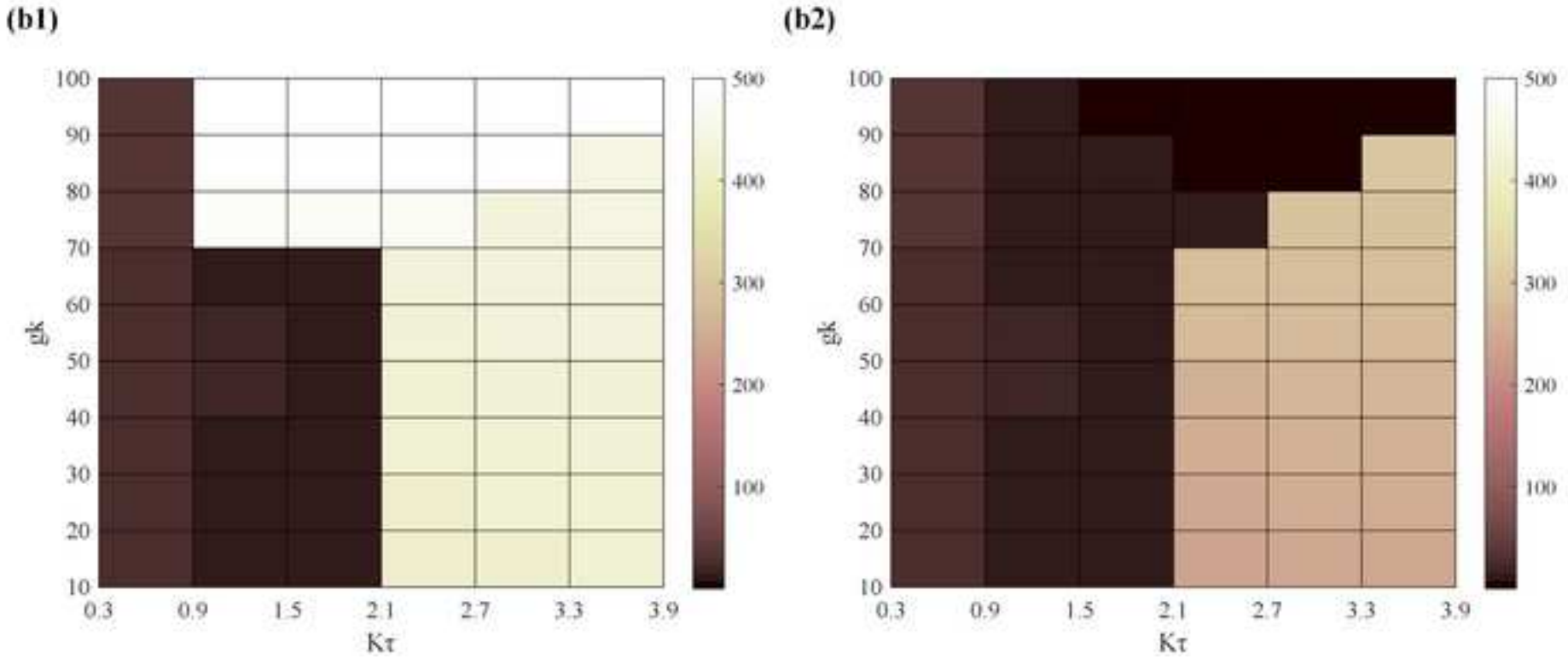

Figure 6(c1)(c2)

Click here to access/download;Figure;Figure 6(c1)(c2).tif

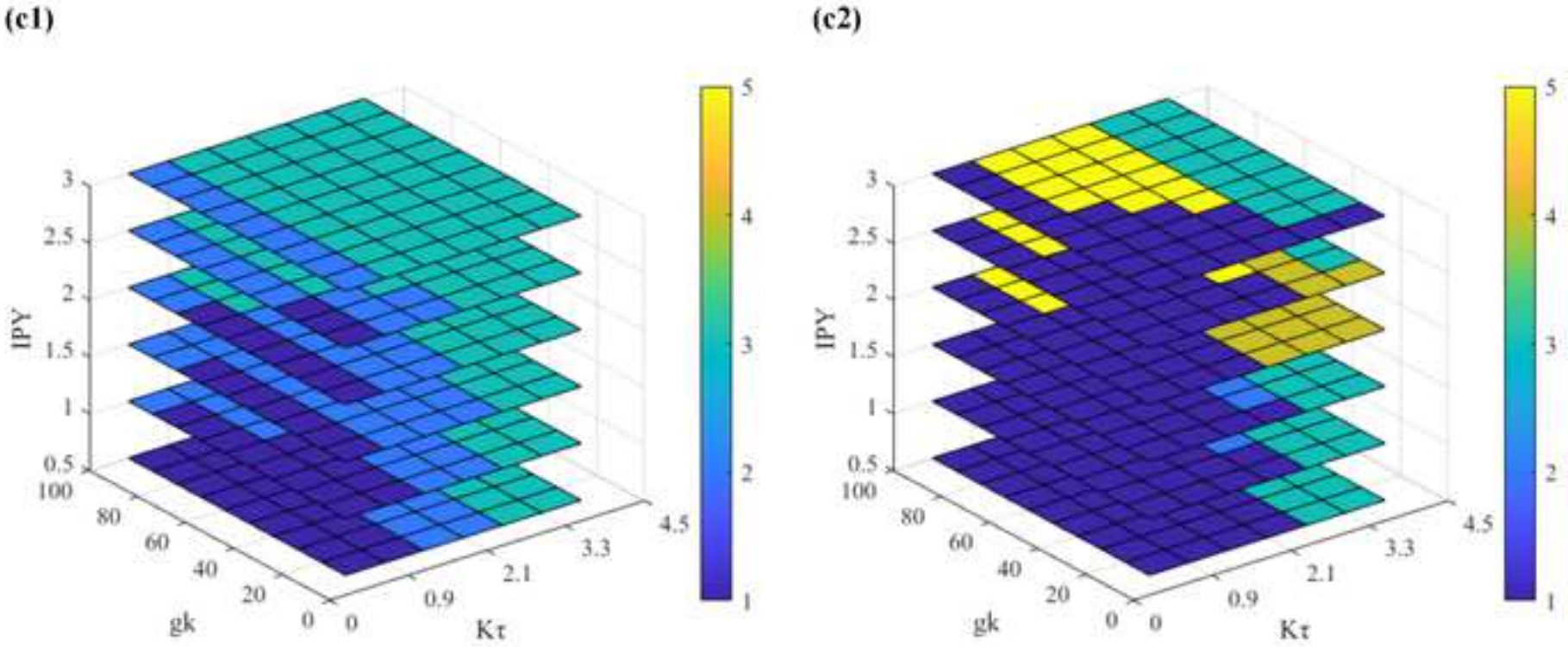

Figure 7(a1)(a2)

Click here to access/download;Figure;Figure 7(a1)(a2).tif

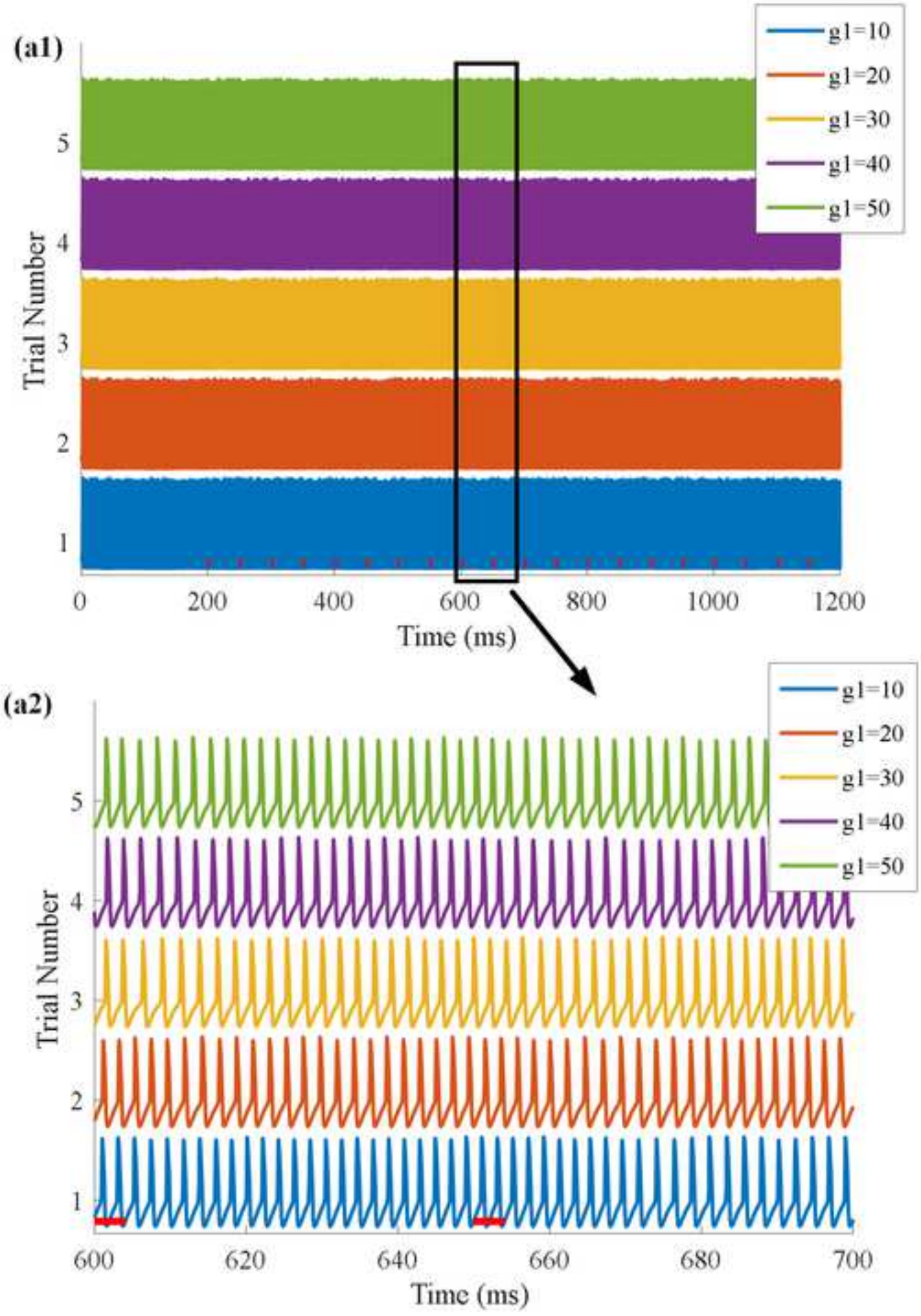

Figure 7(b1)(b2) Click here to access/download;Figure;Figure 7(b1)(b2).tif

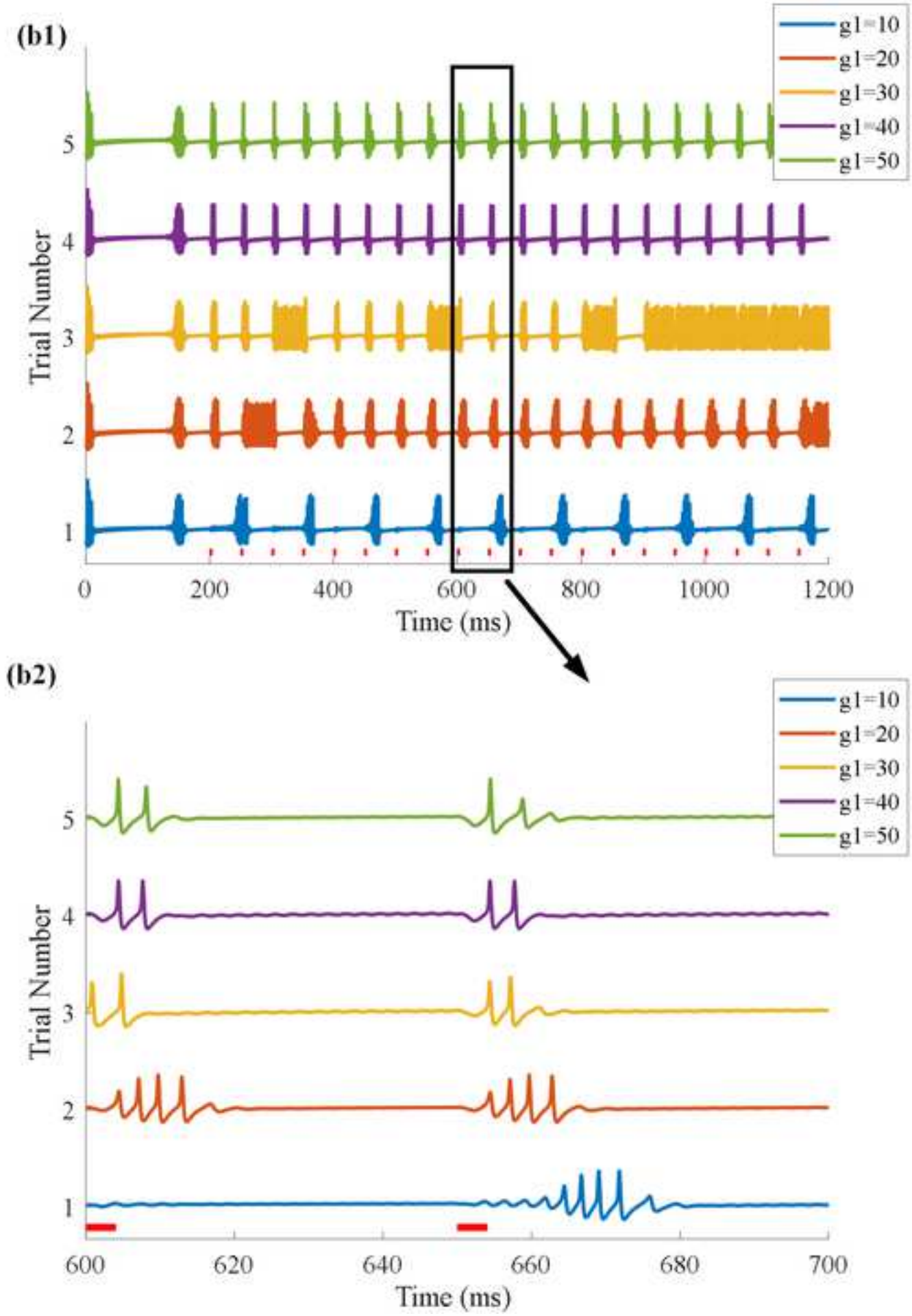

Figure 8

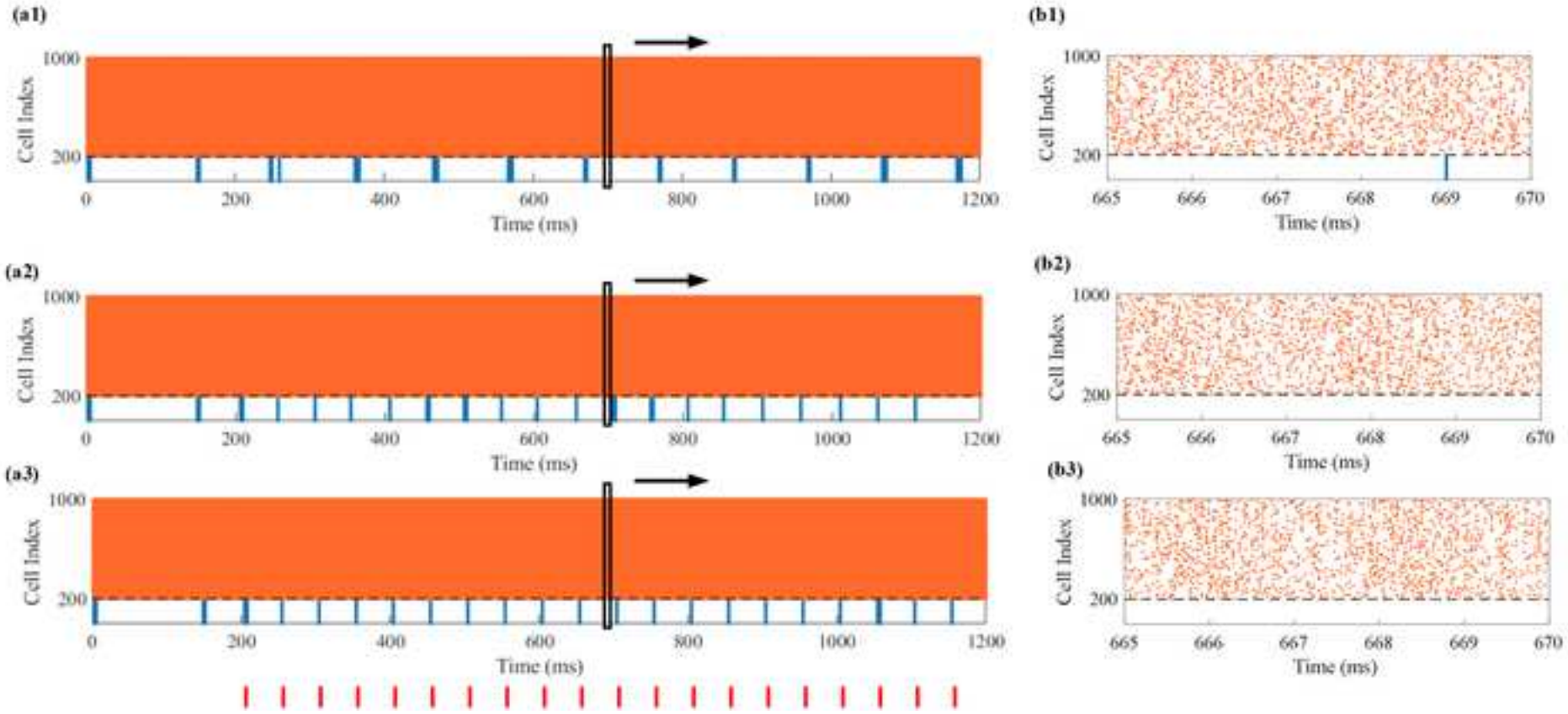

Figure 9(a1)(a2)

Click here to access/download;Figure;Figure 9(a1)(a2).tif

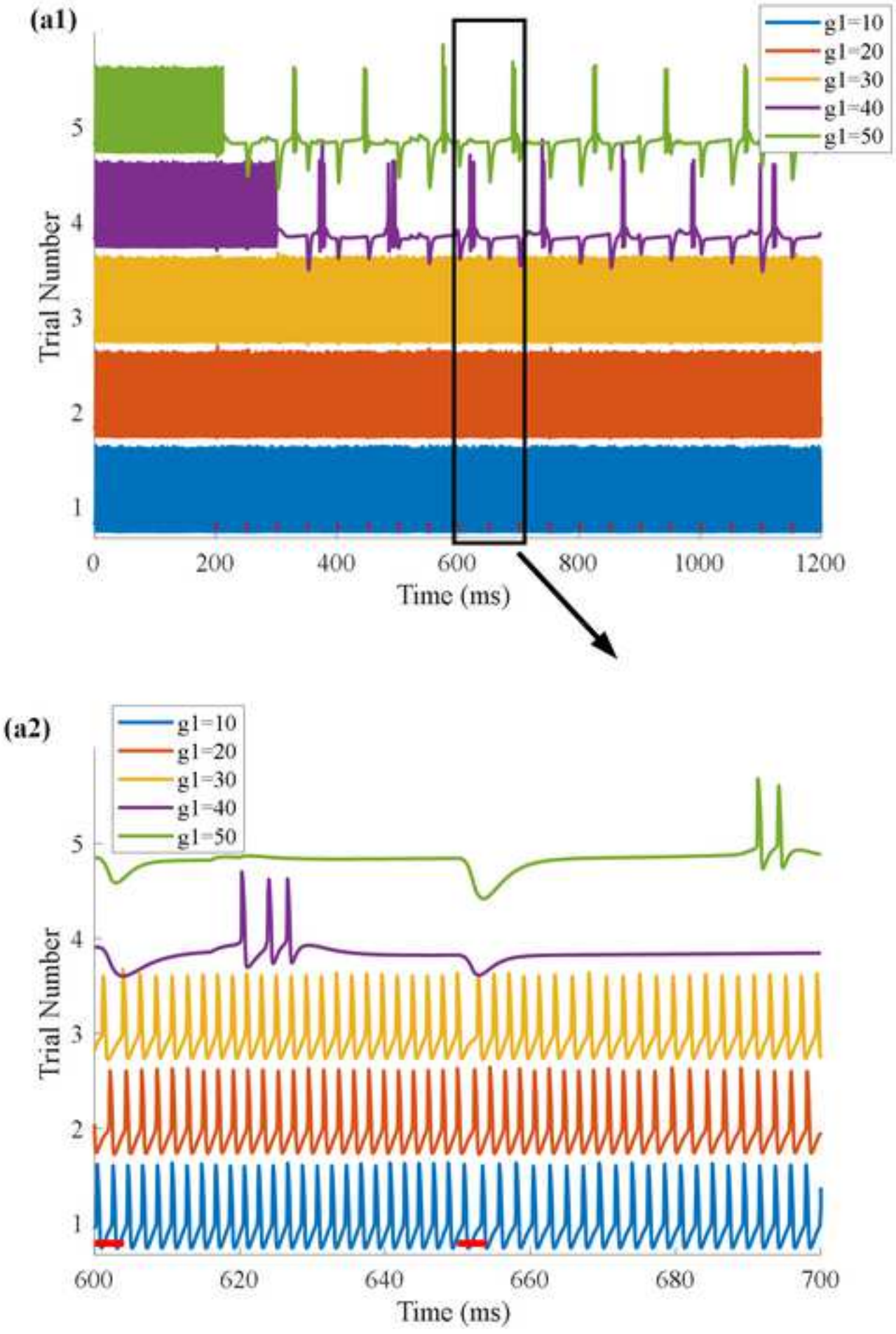

Figure 9(b1)(b2)

Click here to access/download;Figure;Figure 9(b1)(b2).tif

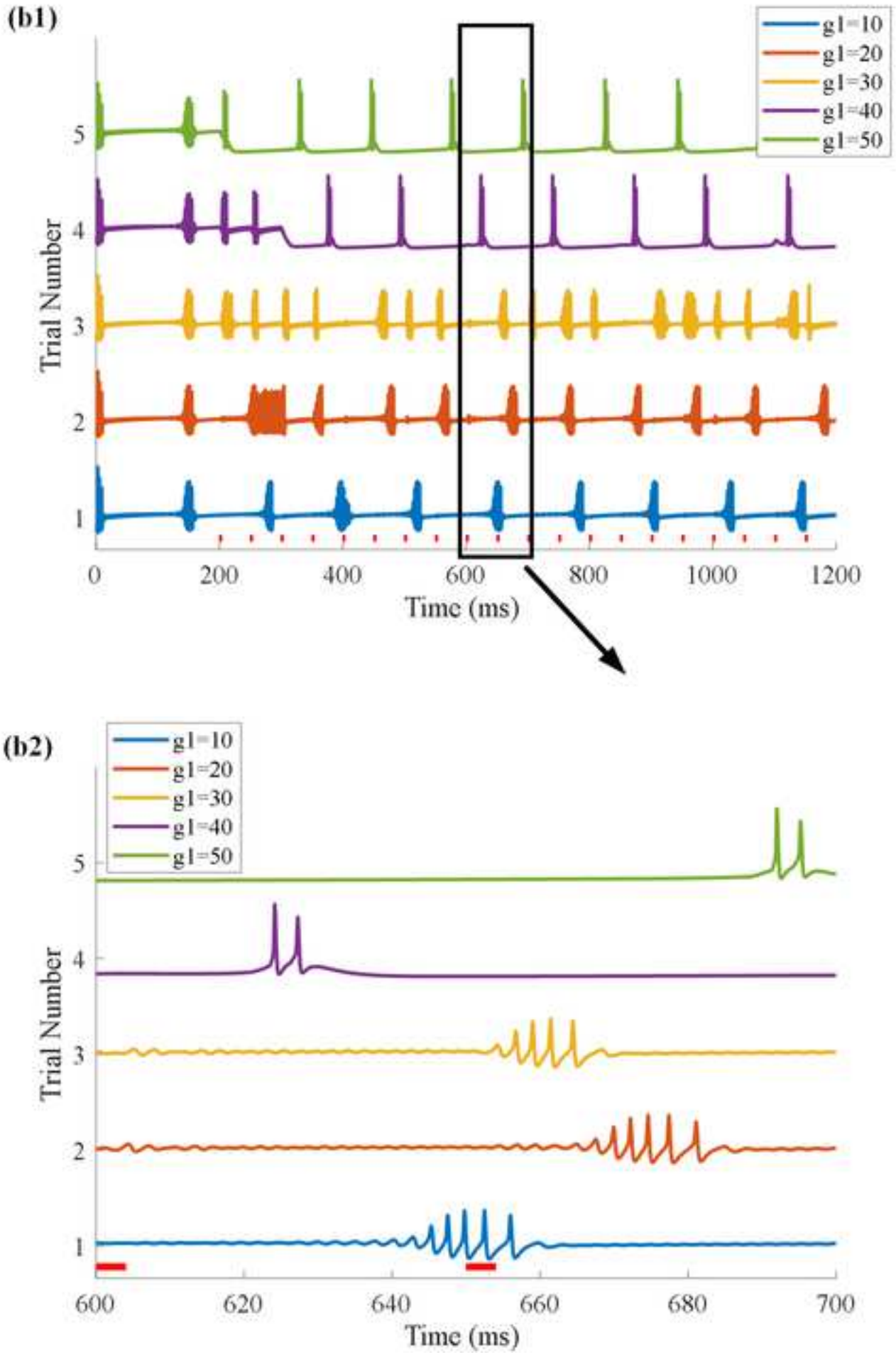

Figure 10

Click here to access/download;Figure;Figure 10.tif

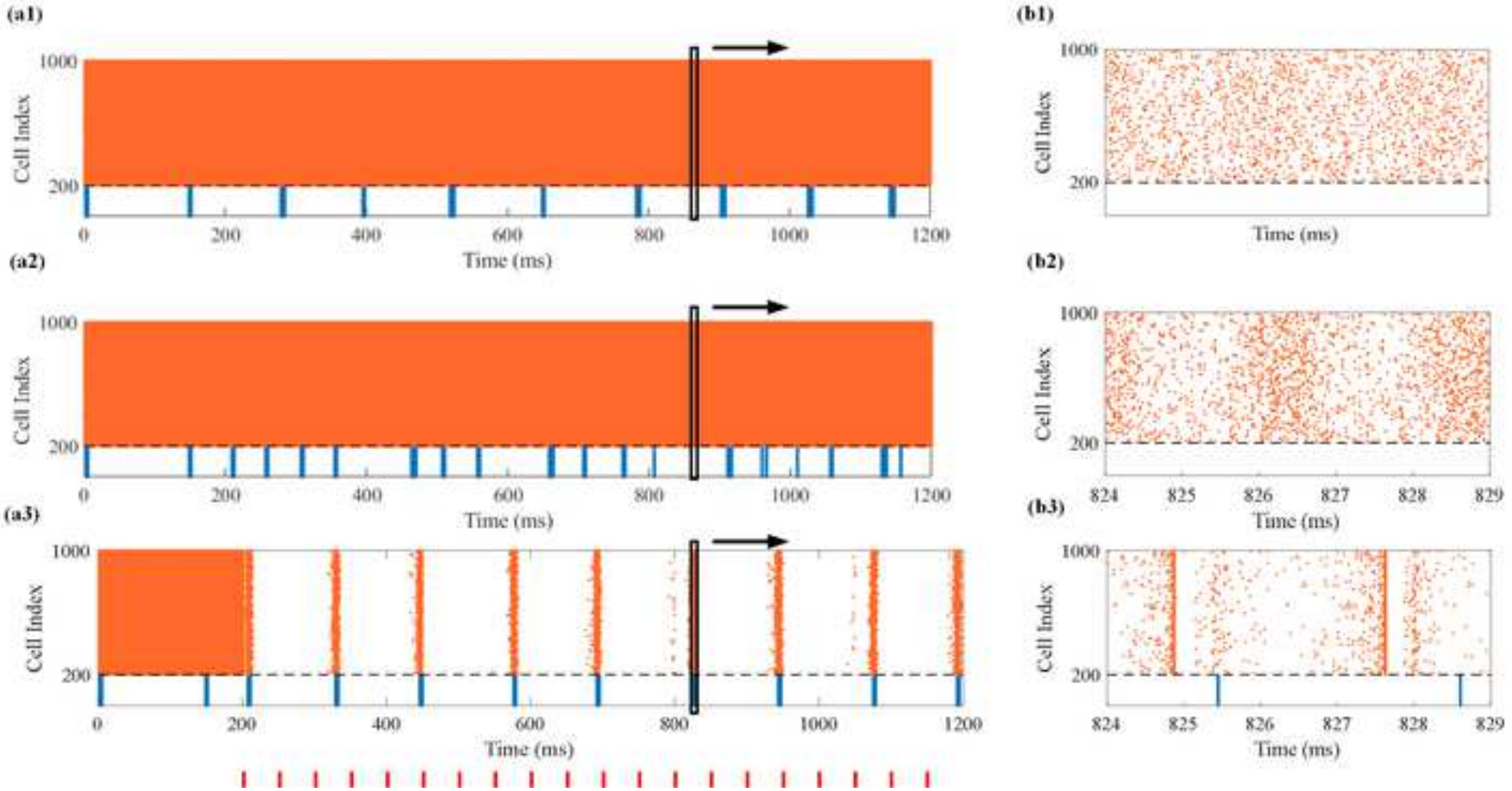

Figure 11